

# Rethinking Sketching as Sampling: A Graph Signal Processing Approach

Fernando Gama, Antonio G. Marques, Gonzalo Mateos, and Alejandro Ribeiro

**Abstract**—Sampling of bandlimited graph signals has well-documented merits for dimensionality reduction, affordable storage, and online processing of streaming network data. Most existing sampling methods are designed to minimize the error incurred when reconstructing the original signal from its samples. Oftentimes these parsimonious signals serve as inputs to computationally-intensive linear operators (e.g., graph filters and transforms). Hence, interest shifts from reconstructing the signal itself towards approximating the output of the prescribed linear operator efficiently. In this context, we propose a novel sampling scheme that leverages the bandlimitedness of the input as well as the transformation whose output we wish to approximate. We formulate problems to jointly optimize sample selection and a sketch of the target linear transformation, so when the latter is affordably applied to the sampled input signal the result is close to the desired output. These designs are carried out off line, and several heuristic solvers are proposed to accommodate high-dimensional problems, especially when computational resources are at a premium. Similar sketching as sampling ideas are also shown effective in the context of linear inverse problems. The developed sampling plus reduced-complexity processing pipeline is particularly useful for data that reside on a low-dimensional subspace and is acquired in a streaming fashion, where the linear transform has to be applied fast and repeatedly to successive inputs or response signals. Numerical tests showing the effectiveness of the proposed algorithms include classification of handwritten digits from as few as 20 out of 784 pixels in the input images and selection of sensors from a network deployed to carry out a distributed parameter estimation task.

**Index Terms**—Sketching, sampling, graph signal processing, streaming, linear transforms, linear inverse problems

## I. INTRODUCTION

Propelled by the desire of analyzing and processing data supported on irregular domains, there has been a growing interest in broadening the scope of traditional signal processing techniques to signals defined on graphs [3], [4]. Noteworthy representatives include sampling of graph signals, linear graph filtering and the graph Fourier transform (GFT) [5], [6], all of them instances of linear problems. This is not surprising since linear models are ubiquitous in science and engineering, due in part to their generality, conceptual simplicity, and mathematical tractability. Along with heterogeneity and lack of regularity, data are increasingly high dimensional and this curse

of dimensionality not only raises statistical challenges, but also major computational hurdles even for linear models [7]. In particular, these limiting factors can hinder processing of streaming data, where say a massive linear operator has to be repeatedly and efficiently applied to a sequence of input (graph) signals [8]. These Big Data challenges motivated a recent body of work collectively addressing so-termed *sketching* problems [9]–[11], which seek computationally-efficient solutions to a subset of (typically inverse) linear problems. The basic idea is to *draw a sketch* of the linear model such that the resulting linear transform is lower dimensional, while still offering quantifiable approximation error guarantees. To achieve this, a fat random projection matrix is designed to pre-multiply and reduce the dimensionality of the linear operator matrix, in such way that the resulting matrix sketch still captures the quintessential structure of the model. The input vector has to be adapted to the sketched operator as well, and to that end the same random projections are applied to the signal in a way often agnostic to the input statistics.

Although random projection methods offer an elegant dimensionality-reduction alternative for several Big Data problems, they face some shortcomings: i) sketching each new input signal entails a nontrivial computational cost, which can be a bottleneck in streaming applications; ii) the design of the random projection matrix does not take into account any a priori information on the input; and iii) the guarantees offered are probabilistic. Alternatively one can think of reducing complexity by simply retaining a few samples of each input. Different from random sketching, under stationarity the sampling can remain fixed and it incurs negligible online complexity. Sampling schemes typically build on a parsimonious model for the signals of interest, often described by a low-dimensional subspace or manifold where data reside. This naturally applies to smooth or bandlimited graph signals admitting a sparse representation in the graph Fourier domain [12]–[15]. However, most existing sampling methods are designed with the objective of reconstructing the original graph signal, and do not account for subsequent processing the signal may undergo; see [16]–[18] for exceptions, the latter two dealing with graph signals.

In this sketching context and towards reducing the online computational cost of obtaining the solution to a linear problem, we propose a novel sampling scheme for signals that belong to a *known* subspace. Since such signals can be conveniently represented as bandlimited graph signals (see Remark 1), we leverage graph signal processing results to build our online schemes. Different from most existing sampling approaches, our design explicitly accounts for the transforma-

Work in this paper is supported by NSF CCF 1750428, NSF CCF 1717120, and ARO W911NF1710438 and Spanish MINECO grants No TEC2013-41604-R and TEC2016-75361-R. F. Gama and A. Ribeiro are with the Dept. of Electrical and Systems Eng., Univ. of Pennsylvania., A. G. Marques is with the Dept. of Signal Theory and Comms., King Juan Carlos Univ., G. Mateos is with the Dept. of Electrical and Computer Eng., Univ. of Rochester. Emails: fgama@seas.upenn.edu, antonio.garcia.marques@urjc.es, gmateosb@ece.rochester.edu, and aribeiro@seas.upenn.edu. Part of the results in this paper were submitted to the 2016 *Asilomar Conf. of Signals, Systems and Computers* [1] and the 2016 *IEEE GobsIP Conf.* [2].

tion whose output we wish to approximate. The approach is then to shift the computational burden to the off-line phase where both the sampling pattern and the sketch of the linear transformation are designed. After doing this only once, the online phase merely consists of repeatedly selecting the signal values dictated by the sampling pattern and processing this stream of samples using the sketch of the linear transformation.

In Sec. II we introduce the mathematical formulation of the direct and inverse linear problems as well as the assumptions on the input (graph) signals. Then, we proceed to present the solutions for the direct and inverse problems in Secs. III and IV, respectively. In both cases, we obtain first a closed form expression for the optimal reduced linear transform as a function of the selected samples of the signal. Then we use that expression to obtain an equivalent optimization problem on the selection of samples, that turns out to be a Semidefinite Program (SDP) modulo binary constraints that arise naturally from the sample (node) selection problem. Sec. V discusses a number of heuristics to obtain tractable solutions to the binary optimization. In Sec. VI we apply this framework to the problem of estimating the graph frequency components of a graph signal in a fast and efficient fashion, as well as to the problems of classifying handwritten digits and selecting sensors. Finally, conclusions are drawn in Sec. VII.

*Notation:* Generically, the entries of a matrix  $\mathbf{X}$  and a (column) vector  $\mathbf{x}$  will be denoted as  $X_{ij}$  and  $x_i$ . The notation  $T$  and  $H$  stands for transpose and transpose conjugate, respectively, and the superscript  $\dagger$  denotes pseudoinverse;  $\mathbf{0}$  is the all-zero vector and  $\mathbf{1}$  is the all-one vector; and the  $\ell_0$  pseudo norm  $\|\mathbf{X}\|_0$  equals the number of nonzero entries in  $\mathbf{X}$ . For a vector  $\mathbf{x}$ ,  $\text{diag}(\mathbf{x})$  is a diagonal matrix with the  $(i, i)$ th entry equal to  $x_i$ ; when applied to a matrix,  $\text{diag}(\mathbf{X})$  is a vector with the diagonal elements of  $\mathbf{X}$ . For vectors  $\mathbf{x}, \mathbf{y} \in \mathbb{R}^n$  we adopt the partial ordering  $\preceq$  defined with respect to the positive orthant  $\mathbb{R}_+^n$  by which a  $\mathbf{x} \preceq \mathbf{y}$  if and only if  $x_i \leq y_i$  for all  $i = 1, \dots, n$ . For symmetric matrices  $\mathbf{X}, \mathbf{Y} \in \mathbb{R}^{n \times n}$ , the partial ordering  $\preceq$  is adopted with respect to the semidefinite cone, by which  $\mathbf{X} \preceq \mathbf{Y}$  if and only if  $\mathbf{Y} - \mathbf{X}$  is positive semi-definite.

## II. PROBLEM FORMULATION

We consider here linear sketching problems for a collection of signals  $\{\mathbf{x}_t\}_{t \in \mathbb{N}}$  that are assumed to belong to a linear subspace or, equivalently, that are assumed to be bandlimited in a graph. The overall idea is to regard  $\{\mathbf{x}_t\}_{t \in \mathbb{N}}$  as realizations of a given random process and leverage the bandlimited assumption to reduce the number of samples required to process the signals of interest. For a precise problem formulation let  $\mathcal{G} = (\mathcal{V}, \mathcal{E}, \mathcal{W})$  be a graph described by a set of  $n$  nodes  $\mathcal{V}$ , a set  $\mathcal{E}$  of edges  $(i, j)$  and a weight function  $\mathcal{W} : \mathcal{E} \rightarrow \mathbb{R}$  that assigns weights to the directed edges. A signal  $\mathbf{x} \in \mathbb{R}^n$  can be defined on the nodes of such a network where each element of the vector  $\mathbf{x} = [x_1, \dots, x_n]^T$  represents a real value present at the node [3], [19]. In order to capture the structure of the network and its impact on the signal, a graph-shift operator  $\mathbf{S} \in \mathbb{R}^{n \times n}$  is introduced [20]. Matrix  $\mathbf{S}$  is such that  $[\mathbf{S}]_{i,j} = 0$  whenever  $i \neq j$ ,  $(j, i) \notin \mathcal{E}$ . The graph shift operator here is considered to be a normal matrix so that we can write

$$\mathbf{S} = \mathbf{V}\mathbf{\Lambda}\mathbf{V}^H = \mathbf{V}\text{diag}([\lambda_1, \dots, \lambda_n]^T)\mathbf{V}^H, \quad (1)$$

where  $\mathbf{V} = [\mathbf{v}_1, \dots, \mathbf{v}_n] \in \mathbb{C}^{n \times n}$  in (1) contains the eigenvectors of  $\mathbf{S}$  and the diagonal matrix  $\mathbf{\Lambda} = \text{diag}([\lambda_1, \dots, \lambda_n]^T) \in \mathbb{C}^{n \times n}$  the corresponding eigenvalues. Since the matrix  $\mathbf{V}$  is unitary it holds  $\mathbf{V}^{-1} = \mathbf{V}^H$ . Examples of normal graph shift operators are the adjacency matrices of some graphs and the Laplacian of any undirected graph, and their respective normalized counterparts [21].

The definition of a graph shift operator  $\mathbf{S}$  serves the purpose of relating the graph signal  $\mathbf{x}$  with the underlying graph topology that models pairwise relationships between signal elements. Here we formalize this link through the definition of a graph Fourier transform (GFT). The GFT is defined as the linear projection of the graph signal  $\mathbf{x}$  onto the eigenvectors of the graph shift operator, obtaining an alternative representation of the signal that is related to the underlying topology. More formally, the GFT of a graph signal  $\mathbf{x}$  is given by  $\tilde{\mathbf{x}} = \mathbf{V}^H \mathbf{x}$  and its inverse  $\mathbf{x} = \mathbf{V}\tilde{\mathbf{x}}$ ; see, e.g., [6]. The inverse (i)GFT is clearly a proper inverse since we can always write

$$\mathbf{x} = \mathbf{V}\tilde{\mathbf{x}} = \mathbf{V}(\mathbf{V}^H \mathbf{x}). \quad (2)$$

The elements of the vector  $\tilde{\mathbf{x}} = [\tilde{x}_1, \dots, \tilde{x}_n]^T \in \mathbb{C}^n$  are said to be the frequency coefficients of the signal  $\mathbf{x}$ . We think of the iGFT relationship  $\mathbf{x} = \mathbf{V}\tilde{\mathbf{x}}$  as an alternative representation of  $\mathbf{x}$  tailored to the graph structure (encoded in  $\mathbf{S}$ ).

Throughout this paper we model the signals  $\{\mathbf{x}_t\}_{t \in \mathbb{N}}$  as (i) being realizations of a zero-mean random process  $\mathbf{x}$ , and (ii) being *bandlimited* in  $\mathbf{S}$ . Formally, we assume that (i)  $\mathbb{E}[\mathbf{x}] = \mathbf{0}$  and  $\mathbf{R}_x = \mathbb{E}[\mathbf{x}\mathbf{x}^T]$ , and (ii) there exists a constant  $k \ll n$  such that  $\tilde{x}_{k'} = 0$  for all  $k' > k$ . We can then define the vector  $\tilde{\mathbf{x}}_k = [\tilde{x}_1, \dots, \tilde{x}_k]^T$  containing the first  $k$  elements of  $\tilde{\mathbf{x}}$  to write the GFT  $\tilde{\mathbf{x}} = [\tilde{\mathbf{x}}_k^T, \mathbf{0}_{n-k}^T]^T$  as the stacking of  $\tilde{\mathbf{x}}_k$  and the all-zero vector of size  $n - k$ . If this is the case, we can group the first  $k$  eigenvectors of  $\mathbf{S}$  in the matrix  $\mathbf{V}_k = [\mathbf{v}_1, \dots, \mathbf{v}_k] \in \mathbb{C}^{n \times k}$  and rewrite (2) as

$$\mathbf{x} = \mathbf{V}_k \tilde{\mathbf{x}}_k = [\mathbf{V}_k, \mathbf{0}_{n-k}] \tilde{\mathbf{x}} = [\mathbf{V}_k, \mathbf{0}_{n-k}] (\mathbf{V}^H \mathbf{x}). \quad (3)$$

The bandlimitedness of  $\mathbf{x}$  also shows up in its statistical description. More precisely, we can use (3) to rewrite  $\mathbf{R}_x = \mathbf{V}_k \mathbb{E}[\tilde{\mathbf{x}}_k \tilde{\mathbf{x}}_k^H] \mathbf{V}_k^H = \mathbf{V}_k \mathbf{T} \mathbf{V}_k^H$ , where  $\mathbf{T} \in \mathbb{C}^{k \times k}$  is the so-called frequency template defined as

$$\mathbf{T} = \mathbb{E}[\tilde{\mathbf{x}}_k \tilde{\mathbf{x}}_k^H]. \quad (4)$$

If no information is available about the process  $\mathbf{x}$  other than it being bandlimited, one can assume  $\tilde{\mathbf{x}}_k$  to be white [22], so that the template is  $\mathbf{T} = \mathbf{I}_k$ , i.e., the identity matrix of size  $k \times k$ . Identity and diagonal templates arise naturally if we assume that  $\mathbf{x}$  is stationary with respect to the shift operator  $\mathbf{S}$ ; see [23]–[25]. Regardless of the color of the template, it follows that the covariance matrix  $\mathbf{R}_x$  is *singular* because the rank of  $\mathbf{T}$  (hence, the rank of  $\mathbf{R}_x$ ) is at most  $k$ .

Another key implication of  $\mathbf{x}$  being bandlimited in  $\mathbf{S}$  is that it can be perfectly recovered from  $k$  samples. These  $k$  samples can be a selection of values at  $k$  nodes [12], a selection of values following from the local aggregation of a diffusion process on  $\mathbf{S}$  at a single node [13], or a combination of both strategies [26]. In either case, a parsimonious equivalent description of  $\mathbf{x}$  becomes available and can be used to process

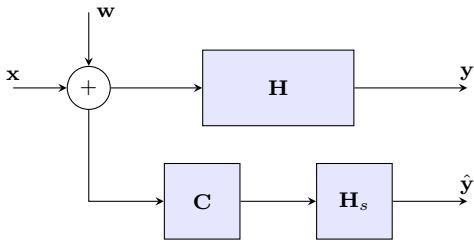


Figure 1. Direct sketching problem. Knowing the linear transform matrix  $\mathbf{H}$  and having access to a stream of noisy inputs  $(\mathbf{x} + \mathbf{w})$ , we want to estimate fast the output  $\mathbf{y}$  of this system, reducing the online computational cost by operating with the matrix sketch  $\mathbf{H}_s$  only on  $p$  samples selected by the selection matrix  $\mathbf{C}$ ,  $\hat{\mathbf{y}} = \mathbf{H}_s \mathbf{C}(\mathbf{x} + \mathbf{w})$ .

$\mathbf{x}$  with a much smaller computational cost if  $k \ll n$ . In this paper we exploit this observation to reduce the computational cost of implementing a very fat linear transformation and to reduce the computational cost of implementing a very tall inverse linear transformation. We introduce these problems in the following section.

**Remark 1 (Bandlimitedness and subspace models).** While (3) is derived under the assumption that  $\mathbf{x}$  is a bandlimited graph signal, the expression holds true for *any* signal  $\mathbf{x}$  belonging to a signal subspace  $\mathcal{X}_k$  of dimension  $k$ . In fact, with  $\mathbf{V}_k$  being an orthonormal basis of  $\mathcal{X}_k$  and defining the matrix  $\mathbf{P}_{\mathcal{X}_k} = \mathbf{V}_k \mathbf{V}_k^H$ , which projects any input signal into  $\mathcal{X}_k$ , it follows readily that (3) can be written as  $\mathbf{x} = \mathbf{P}_{\mathcal{X}_k} \mathbf{x}$ , demonstrating that our bandlimited signals can be equivalently thought as signals lying on  $\mathcal{X}_k$ . Although the exposition in this section assumed that the graph shift operator  $\mathbf{S}$  was known and used  $\mathbf{S}$  to find  $\mathbf{V}_k$  and  $\mathcal{X}_k$ , one can also follow the reverse path and use  $\mathcal{X}_k$  to find first  $\mathbf{V}_k$  and then  $\mathbf{S}$ . Schemes to identify  $\mathbf{S}$  based on  $\mathbf{V}_k$  have been reported in [27], [28].

#### A. Linear sketching problems

We start by formulating the optimal direct and inverse sketching problems and then discuss a suboptimal design.

1) *Direct sketching problem:* The setup of the *direct* linear sketching problem is illustrated in Fig. 1. We are given a known matrix  $\mathbf{H} \in \mathbb{R}^{m \times n}$  and observe a possibly noisy realization of a signal  $\mathbf{x}$  that is bandlimited in the graph shift  $\mathbf{S}$  with spectral template  $\mathbf{T}$ . The goal is to compute an estimate of the output of the linear transformation  $\mathbf{y} = \mathbf{H}\mathbf{x}$ . As an interesting aside, the fact of  $\mathbf{x}$  being bandlimited in  $\mathbf{S}$  dictates that the optimal transformation can be written as a low-pass filter on the graph  $\mathbf{S}$ , followed by a lower dimensional linear transformation. Assuming that these two steps are combined into a single one, their computational cost is of order  $O(mn)$ . Our operating assumption, however, implies that it is possible to represent  $\mathbf{x}$  with  $k \ll n$  samples. We therefore proceed through the alternative route of first drawing  $p \geq k$  samples from the signal  $\mathbf{x}$  to yield the sampled signal  $\mathbf{C}\mathbf{x}$ , where  $\mathbf{C}$  is a  $p \times n$  sampling matrix that selects  $p$  out of the  $n$  elements of  $\mathbf{x}$ . To process the reduced-dimensionality sampled input, the goal is to optimally design a sketch  $\mathbf{H}_s \in \mathbb{R}^{m \times p}$  of the linear transform  $\mathbf{H}$ , so that  $\hat{\mathbf{y}} = \mathbf{H}_s \mathbf{C}\mathbf{x}$  is an accurate estimate of the intended transformation  $\mathbf{y} = \mathbf{H}\mathbf{x}$ . Given  $\mathbf{H}_s$  and  $\mathbf{C}$ , the cost of forming  $\hat{\mathbf{y}}$  is of order  $O(mp)$  because the sampled vector

$\mathbf{C}\mathbf{x}$  contains  $p$  elements only. The computational cost is then reduced by a factor  $p/n$ , which can be substantial if we select  $k \leq p \ll n$ .

For a formal problem statement let us begin by defining the set  $\mathcal{C}_{pn}$  of admissible  $p \times n$  sampling matrices  $\mathbf{C}$ , for given  $p$  and  $n$ . Such matrices must have binary elements  $C_{ij} \in \{0, 1\}$  and be such that each row contains *exactly* one nonzero element while each column contains *at most* one nonzero element. Accordingly, the set of all matrices of this form is given by

$$\mathcal{C}_{pn} := \{ \mathbf{C} \in \{0, 1\}^{p \times n} : \mathbf{C}\mathbf{1} = \mathbf{1}, \mathbf{C}^T \mathbf{1} \preceq \mathbf{1}, \}. \quad (5)$$

For upcoming derivations it is important to observe that selection matrices  $\mathbf{C} \in \mathcal{C}_{pn}$  have rank  $p$  and satisfy  $\mathbf{C}\mathbf{C}^T = \mathbf{I}_p$ . The selection matrix also satisfies  $\mathbf{C}^T \mathbf{C} = \text{diag}(\mathbf{c})$ , meaning that  $\mathbf{C}^T \mathbf{C}$  is a diagonal matrix and vector  $\mathbf{c} \in \{0, 1\}^n$  collects its diagonal elements, where  $c_i = 1$  if and only if the  $i$ -th column of  $\mathbf{C}$  contains a one, or, equivalently, if the  $i$ -th element of  $\mathbf{x}$  is sampled. Consequently, there is a one-to-one correspondence between the sampling matrix  $\mathbf{C}$  and the sampling vector  $\mathbf{c}$ , modulo the ordering of the rows in  $\mathbf{C}$ .

When the input signal is corrupted by additive noise  $\mathbf{w}$  the sampled signal is  $\mathbf{C}(\mathbf{x} + \mathbf{w})$ ; see Fig. 1. After processing the samples with the linear transformation  $\mathbf{H}_s$ , we obtain the estimate  $\hat{\mathbf{y}} = \mathbf{H}_s \mathbf{C}(\mathbf{x} + \mathbf{w})$ . Our goal here is to find a sampling matrix  $\mathbf{C}$  and a sketch  $\mathbf{H}_s \in \mathbb{R}^{m \times p}$  that minimizes the mean-squared error (MSE) with respect to the desired response  $\mathbf{y} = \mathbf{H}\mathbf{x}$ . We are therefore searching for the matrices  $\mathbf{C}^*$  and  $\mathbf{H}_s^*$  that solve the non-convex optimization problem

$$\{ \mathbf{C}^*, \mathbf{H}_s^* \} := \underset{\mathbf{C} \in \mathcal{C}_{pn}, \mathbf{H}_s}{\text{argmin}} \mathbb{E} \left[ \left\| \mathbf{H}_s \mathbf{C}(\mathbf{x} + \mathbf{w}) - \mathbf{H}\mathbf{x} \right\|_2^2 \right]. \quad (6)$$

We emphasize here that solving (6) is costly, indeed, intractable due to the binary constraints  $\mathbf{C} \in \mathcal{C}_{pn}$ . Methods for approximately solving (6) with manageable cost are presented in Sec. V, but these approaches still incur a cost much higher than just evaluating the linear transformation  $\mathbf{y} = \mathbf{H}\mathbf{x}$ . As pointed out in the introduction, the operating assumption in this work is that the optimization in (6) is carried out off line and only once, whereas during online operation we are presented with a stream of bandlimited signals  $\{\mathbf{x}_t\}_{t \in \mathbb{N}}$ . While the original goal is to process each of those signals with the transformation  $\mathbf{H}$  [29], through the proposed sampling plus reduced-complexity processing pipeline, for every  $t$  we first sample  $\mathbf{x}_t$  according to  $\mathbf{C}^*$  and then apply the sketch  $\mathbf{H}_s^*$  to the sampled signal  $\mathbf{C}^* \mathbf{x}_t$ , reducing the online operational cost by a factor of  $p/n$ . See Sec. III for a thorough treatment of the direct problem.

2) *Inverse sketching problem:* The basic setting for the related linear *inverse* sketching problem is illustrated in Fig. 2. We are again given a matrix  $\mathbf{H} \in \mathbb{R}^{m \times n}$  and we have access to possibly noisy realizations of the output  $\mathbf{x}$  of the system  $\mathbf{x} = \mathbf{H}^T \mathbf{y}$ . These realizations are also bandlimited in the graph shift  $\mathbf{S}$  and have a spectral template  $\mathbf{T}$ . In this case, we aim at estimating the input  $\mathbf{y}$  that generated the observed output  $\mathbf{x} = \mathbf{H}^T \mathbf{y}$ . If  $\mathbf{H}$  is full rank, then the ordinary least squares (LS) estimator of  $\mathbf{y}$  is given by

$$\hat{\mathbf{y}}_{\text{LS}} = \mathbf{A}_{\text{LS}} \mathbf{x}, \quad \text{with } \mathbf{A}_{\text{LS}} = (\mathbf{H}\mathbf{H}^T)^{-1} \mathbf{H}. \quad (7)$$

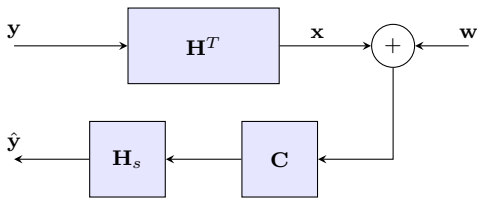


Figure 2. Inverse sketching problem. Given knowledge of the linear transform matrix  $\mathbf{H}^T$  and having access to a stream of noisy observations of the output ( $\mathbf{x} + \mathbf{w}$ ), we want to estimate the input  $\mathbf{y}$  generating such outputs in a way that minimizes the online computational cost. This is achieved by designing a matrix sketch  $\mathbf{H}_s$  that operates on selected samples of the measured output  $\mathbf{C}(\mathbf{x} + \mathbf{w})$ .

Computing matrix  $\mathbf{A}_{\text{LS}}$  demands  $O(mn^2)$  calculations and its application to the output in order to estimate the input entails additional  $mn$  operations [30]. Under the assumption that  $\mathbf{x}$  is bandlimited and can thus be represented with  $k \ll n$  samples, an alternative procedure is to first design an appropriate sketch of  $\mathbf{x}$  and matrix  $\mathbf{A}_{\text{LS}}$ . This way, an estimate  $\hat{\mathbf{y}}$  can be obtained by sampling the output and applying it to a sketch  $\mathbf{H}_s \in \mathbb{R}^{m \times p}$  of the inverse mapping. More formally, given noisy observations of the output  $\mathbf{x} + \mathbf{w}$ , we want to form an estimator of the input  $\hat{\mathbf{y}} = \mathbf{H}_s \mathbf{C}(\mathbf{x} + \mathbf{w})$  that minimizes the MSE between the predicted response  $\mathbf{H}^T \hat{\mathbf{y}}$  and the actual one  $\mathbf{x} = \mathbf{H}^T \mathbf{y}$ . The optimum pair  $\{\mathbf{C}^*, \mathbf{H}_s^*\}$  is thus given by

$$\{\mathbf{C}^*, \mathbf{H}_s^*\} := \underset{\mathbf{C} \in \mathcal{C}_{pn}, \mathbf{H}_s}{\operatorname{argmin}} \mathbb{E} \left[ \|\mathbf{H}^T \mathbf{H}_s \mathbf{C}(\mathbf{x} + \mathbf{w}) - \mathbf{x}\|_2^2 \right]. \quad (8)$$

Again, solving (8) is in general intractable, and even natural relaxations can be computationally expensive. However, recall that the streaming setting considered here calls for repetitive application of the inverse mapping  $\mathbf{A}_{\text{LS}}$ , a task which incurs  $O(mn)$  cost per datum. Thus, having available a sketch  $\mathbf{H}_s$  that is applied only to a subset of  $p$  samples of  $\mathbf{x}$  speeds up the online computation of the solution by a factor of  $O(n/p)$ . This inverse problem is addressed in Section IV.

3) *Operator sketching via row or column sampling*: There may be applications where the sketch  $\mathbf{H}_s$  must obey additional constraints. This can be the case in distributed setups where the values of  $\mathbf{H}$  cannot be adapted or when the calculation (or storage) of the optimal  $\mathbf{H}_s$  is impossible. In those setups, a design of a suboptimal sketch  $\mathbf{H}_s$  based directly on the original values of  $\mathbf{H}$  – e.g., via sampling of its rows or columns – may be the only alternative. To be more specific, consider first the case of the direct problem where  $\mathbf{y} = \mathbf{H}\mathbf{x}$ . Then, selecting  $\mathbf{C}$  will not only determine the reduced input as  $\mathbf{C}\mathbf{x}$  but also the sketch as  $\mathbf{H}_s = \mathbf{H}\mathbf{C}^T$  – i.e., the columns of  $\mathbf{H}$  corresponding to the selected samples –, so that the estimated output will be  $\hat{\mathbf{y}} = \mathbf{H}\mathbf{C}^T \mathbf{C}\mathbf{x}$ . Likewise in the inverse problem, sampling the output  $\mathbf{x}$  amounts also to selecting columns of  $\mathbf{H}$ . Although these more constrained sampling-sketching designs will give rise to a lower performance, they can be nevertheless optimized. The details can be found in Secs. III-B and IV-B.

## B. Sketching and sampling

The problems stated in the previous section are related to both sampling of graph signals and (traditional) matrix sketching [10], [11]. To position the contributions of our work in context, here we elaborate on this important connection.

In the context of linear inverse problems, the objective of traditional sketching techniques is to reduce the dimension of the linear transformation  $\mathbf{H}^T$  so that the number of computations required for obtaining an estimate of  $\mathbf{y}$  is reduced [10], [11]. The sketching matrix  $\mathbf{K} \in \mathbb{R}^{p \times n}$ , with  $p \ll n$ , is designed such that the compressed quantities  $\mathbf{K}\mathbf{H}^T \in \mathbb{R}^{p \times m}$  and  $\mathbf{K}\mathbf{x} \in \mathbb{R}^p$  can be calculated fast. Given  $\mathbf{K}$ , an approximate solution to the (inverse) problem can be found as

$$\hat{\mathbf{y}}_s = \min_{\mathbf{y}} \|(\mathbf{K}\mathbf{H}^T)\mathbf{y} - (\mathbf{K}\mathbf{x})\|_2^2,$$

which is given in closed form as  $\hat{\mathbf{y}}_s = (\mathbf{K}\mathbf{H}^T \mathbf{H}\mathbf{K}^T)^{-1} \mathbf{K}\mathbf{x}$ . The sketching matrix  $\mathbf{K}$  is (usually) random and need not be sparse, although it must have a special structure that facilitates its efficient multiplication with  $\mathbf{H}^T$  and  $\mathbf{x}$ . It is important to observe that within this approach there is no particular distinction between the off-line cost of computing  $\mathbf{K}\mathbf{H}^T$  and the online cost of computing  $\mathbf{K}\mathbf{x}$ . If efficient online operation is the major concern, evaluating  $\mathbf{K}\mathbf{x}$  is fastest when adopting a selection matrix  $\mathbf{K} := \mathbf{C} \in \mathcal{C}_{pn}$ . However, according to these traditional sketching techniques, selecting samples of  $\mathbf{x}$  using  $\mathbf{C}$  would imply also a selection (of columns) of  $\mathbf{H}$  as  $\mathbf{C}\mathbf{H}^T$ , which prevents an optimum (off-line) design of  $\mathbf{H}_s$  (cf. the third problem outlined in Section II-A). Finally, note also that traditionally  $\mathbf{K}$  is constructed as a so-termed random projection matrix. This facilitates – by leveraging the celebrated Johnson-Lindenstrauss lemma [31] – providing *probabilistic* approximation guarantees that depend on the number  $p$  of samples taken.

On the other hand, (selection) sampling picks a subset of  $p$  elements of  $\mathbf{x}$  in such a way that, if the graph signal is bandlimited with bandwidth  $k$ , then it can be exactly reconstructed from the selected samples –the value of the signal at only  $p \geq k$  nodes [12], [15]. In essence, a selection matrix  $\mathbf{C} \in \mathcal{C}_{pn}$  is designed in such a way that  $\mathbf{C}\mathbf{x}$  contains enough information for accurately recovering the whole signal  $\mathbf{x}$  via suitable interpolation of these samples [32]. In the noiseless case, any  $\mathbf{C}$  with  $p \geq k$  that satisfies that  $\mathbf{C}\mathbf{V}_k$  is full rank suffices, and perfect recovery is guaranteed by

$$\mathbf{x} = \mathbf{V}_k (\mathbf{C}\mathbf{V}_k)^\dagger (\mathbf{C}\mathbf{x}). \quad (9)$$

In the noisy case, there are several methods and algorithms for obtaining the optimal selection matrix  $\mathbf{C}$ , see [12], [13]. Selection sampling of  $\mathbf{x}$  is particularly useful for compression and storage in the context of streaming data.

All in all, existing sampling schemes consider the properties of  $\mathbf{x}$  with the sole objective of signal reconstruction. Accordingly, they are agnostic to higher-level tasks for which the sampled signal  $\mathbf{C}\mathbf{x}$  may serve as input. On the other hand, traditional sketching methods neither consider the properties of  $\mathbf{x}$ , nor they anticipate differences in online and off-line computational power (i.e., focus is on batch processing). Hence, they yield suboptimal alternatives when seeking for an approximate solution with low computational cost in the online phase. This motivates the approach in this paper, which takes into account the information of  $\mathbf{x}$  and  $\mathbf{H}$  jointly.

## III. DIRECT SKETCHING AS GRAPH SIGNAL SAMPLING

After introducing notation and presenting the problem formulation (cf. Fig. 1 and Section II-A1), the focus in this

section is on describing the optimal sampling and sketching solutions for the direct problem.

We start by analyzing the solution for the case where the observations are noise free (i.e.,  $\mathbf{w} = \mathbf{0}$  in Fig. 1). This will be useful to gain insights on the solution to the noisy formulation as well as to derive heuristics to approximate the output of the linear transform. Since in this noiseless scenario we have that  $\mathbf{w} = \mathbf{0}$ , then the desired output is  $\mathbf{y} = \mathbf{H}\mathbf{x}$  and the reduced-complexity approximation is given by  $\hat{\mathbf{y}} = \mathbf{H}_s\mathbf{C}\mathbf{x}$ . The following result asserts that perfect estimation is possible, namely that  $\hat{\mathbf{y}} = \mathbf{y}$  if the number of samples is  $p \geq k$ .

**Proposition 1.** *Let  $\mathbf{x} \in \mathbb{R}^n$  be a  $k$ -bandlimited signal with known spectral template  $\mathbf{T} \in \mathbb{C}^{k \times k}$  and let  $\mathbf{H} \in \mathbb{R}^{m \times n}$  be a linear transformation. Let  $\mathbf{H}_s \in \mathbb{R}^{m \times p}$  be a reduced-input dimensionality sketch of  $\mathbf{H}$ ,  $p \leq n$  and  $\mathbf{C} \in \mathcal{C}_{pn}$  be a selection matrix. In the absence of noise ( $\mathbf{w} = \mathbf{0}$ ), if  $p = k$  and  $\mathbf{C}^*$  is designed such that  $\text{rank}\{\mathbf{C}^*\mathbf{V}_k\} = p = k$ , then  $\hat{\mathbf{y}} = \mathbf{H}_s^*\mathbf{C}^*\mathbf{x}$  is equal to the desired output  $\mathbf{y} = \mathbf{H}\mathbf{x}$  provided that the sketch  $\mathbf{H}_s^*$  is given by*

$$\mathbf{H}_s^* = \mathbf{H}\mathbf{V}_k(\mathbf{C}^*\mathbf{V}_k)^{-1}. \quad (10)$$

*Proof.* Since for any two vectors  $\mathbf{u}, \mathbf{v} \in \mathbb{R}^n$  we have  $\mathbf{u}^T\mathbf{v} = \text{tr}[\mathbf{u}^T\mathbf{v}] = \text{tr}[\mathbf{v}\mathbf{u}^T]$ , then the MSE criterion [cf. (6)] becomes

$$\begin{aligned} \mathbb{E} [\|\mathbf{y} - \hat{\mathbf{y}}\|_2^2] &= \mathbb{E} [\|\mathbf{H}\mathbf{x} - \mathbf{H}_s\mathbf{C}\mathbf{x}\|_2^2] \\ &= \text{tr}[\mathbf{H}\mathbf{R}_x\mathbf{H}^T - 2\mathbf{H}_s\mathbf{C}\mathbf{R}_x\mathbf{H}^T + \mathbf{H}_s\mathbf{C}\mathbf{R}_x\mathbf{C}^T\mathbf{H}_s^T]. \end{aligned} \quad (11)$$

Recall that  $\text{rank}\{\mathbf{C}\} = p$  for any  $\mathbf{C} \in \mathcal{C}_{pn}$ . Optimizing the MSE cost over  $\mathbf{H}_s$  first, results in the following identity that  $\mathbf{H}_s^*$  should satisfy (recall  $\mathbf{R}_x = \mathbf{V}_k\mathbf{T}\mathbf{V}_k^H$ )

$$\mathbf{H}\mathbf{V}_k\mathbf{T}\mathbf{V}_k^H\mathbf{C}^T = \mathbf{H}_s^*\mathbf{C}\mathbf{V}_k\mathbf{T}\mathbf{V}_k^H\mathbf{C}^T. \quad (12)$$

Observe that if  $\mathbf{C}$  is chosen such that  $\text{rank}\{\mathbf{C}\mathbf{V}_k\} = k$  (i.e. that the  $p$  selected rows of  $\mathbf{V}_k$  contain a basis for  $\mathbb{C}^k$ ), then  $(\mathbf{V}_k^H\mathbf{C}^T\mathbf{C}\mathbf{V}_k)^{-1}$  exists. Now, consider the  $p \times k$  matrix  $\mathbf{M} = \mathbf{C}\mathbf{V}_k(\mathbf{V}_k^H\mathbf{C}^T\mathbf{C}\mathbf{V}_k)^{-1}\mathbf{T}^{-1}$ . If we set  $p = k$ , then  $\mathbf{M}$  is nonsingular and we can multiply both sides of (12) from the right with  $\mathbf{M}$ , keeping the equivalence between equations. That multiplication yields

$$\mathbf{H}\mathbf{V}_k = \mathbf{H}_s^*\mathbf{C}\mathbf{V}_k.$$

Finally, the fact that  $\text{rank}\{\mathbf{C}\mathbf{V}_k\} = p = k$  guarantees that  $\mathbf{C}\mathbf{V}_k$  is square and nonsingular, so that its inverse exists and can be used to obtain the solution for  $\mathbf{H}_s^*$  given in (10).  $\square$

All in all, in the absence of noise it suffices to first set  $p = k$  to find a selection matrix  $\mathbf{C} \in \mathcal{C}_{pn}$  such that  $\text{rank}\{\mathbf{C}\mathbf{V}_k\} = p = k$ , and then obtain  $\mathbf{H}_s$  as per Proposition 1. This ensures that  $\mathbf{y}$  can be formed error-free using  $p$  samples of  $\mathbf{x}$  via  $\mathbf{y} = \hat{\mathbf{y}} = \mathbf{H}_s\mathbf{C}\mathbf{x}$ . Clearly, selecting  $p \geq k$  will also do the job, provided that  $\text{rank}\{\mathbf{C}\mathbf{V}_k\} = k$ . Before moving on to the noisy setting, a remark is in order.

**Remark 2 (Signal recovery via selection sampling).** Note that  $\text{rank}\{\mathbf{C}\mathbf{V}_k\} = k$  is the same condition for exact signal recovery as with selection sampling [cf. (9)]. Hence, the same techniques proposed in [12] for finding a subset of  $p$  rows of  $\mathbf{V}_k$  that are linearly independent can be used here. This coincidence should not come as a surprise, since in the absence

of noise the design of  $\mathbf{C}$  decouples from that of  $\mathbf{H}_s$ . As a result, existing methods to determine the most informative nodes in sampling scenarios are also applicable here [17].

#### A. Noisy case

Now consider that the noise vector signal  $\mathbf{w} \in \mathbb{R}^n$  is random and independent of  $\mathbf{x}$ , with  $\mathbb{E}[\mathbf{w}] = \mathbf{0}$ ,  $\mathbf{R}_w = \mathbb{E}[\mathbf{w}\mathbf{w}^T] \in \mathbb{R}^{n \times n}$  and  $\mathbf{R}_w \succ \mathbf{0}$ . In this case, we have  $\mathbf{y} = \mathbf{H}\mathbf{x}$  and  $\hat{\mathbf{y}} = \mathbf{H}_s\mathbf{C}(\mathbf{x} + \mathbf{w})$  (see Fig. 1). As a result, the design of  $\mathbf{H}_s$  and  $\mathbf{C}$  to minimize (6) must account for the noise model as well. The joint design of  $\mathbf{H}_s$  and  $\mathbf{C}$  will be addressed as a two-stage optimization that proceeds into three steps: First, the optimal sketch  $\mathbf{H}_s$  is written as a function of  $\mathbf{C}$ . Second, such a function is substituted into the joint optimization to yield a problem that depends only on  $\mathbf{C}$ . Third, the optimal  $\mathbf{H}_s^*$  is found using the function in step one and the optimal value of  $\mathbf{C}^*$  found in the step two. Defining the covariance matrix of the output  $\mathbf{y}$  as  $\mathbf{R}_y = \mathbb{E}[\mathbf{y}\mathbf{y}^T] = \mathbf{H}\mathbf{R}_x\mathbf{H}^T \in \mathbb{R}^{m \times m}$ , the outcome of this process is described in the following proposition.

**Proposition 2.** *The solution of the direct linear sketching problem in the presence of noise (6) is given by  $\mathbf{C}^*$  and  $\mathbf{H}_s^* = \mathbf{H}_s^*(\mathbf{C}^*)$ , where*

$$\mathbf{H}_s^*(\mathbf{C}) = \mathbf{H}\mathbf{R}_x\mathbf{C}^T (\mathbf{C}(\mathbf{R}_x + \mathbf{R}_w)\mathbf{C}^T)^{-1} \quad (13)$$

and  $\mathbf{C}^*$  can be obtained as the solution to the problem

$$\min_{\mathbf{C} \in \mathcal{C}_{pn}} \text{tr} \left[ \mathbf{R}_y - \mathbf{H}\mathbf{R}_x\mathbf{C}^T (\mathbf{C}(\mathbf{R}_x + \mathbf{R}_w)\mathbf{C}^T)^{-1} \mathbf{C}\mathbf{R}_x\mathbf{H}^T \right]. \quad (14)$$

*Proof.* The objective function in (6) can be rewritten as

$$\begin{aligned} \mathbb{E} [\|\mathbf{y} - \hat{\mathbf{y}}\|_2^2] &= \mathbb{E} [\|\mathbf{H}\mathbf{x} - \mathbf{H}_s\mathbf{C}(\mathbf{x} + \mathbf{w})\|_2^2] \\ &= \text{tr} [\mathbf{H}\mathbf{R}_x\mathbf{H}^T - 2\mathbf{H}_s\mathbf{C}\mathbf{R}_x\mathbf{H}^T + \mathbf{H}_s\mathbf{C}(\mathbf{R}_x + \mathbf{R}_w)\mathbf{C}^T\mathbf{H}_s^T] \end{aligned} \quad (15)$$

since  $\mathbf{x}$  and  $\mathbf{w}$  are assumed independent. Optimizing with respect to  $\mathbf{H}_s$  first, yields

$$\mathbf{H}_s^*(\mathbf{C}) = \mathbf{H}\mathbf{R}_x\mathbf{C}^T (\mathbf{C}(\mathbf{R}_x + \mathbf{R}_w)\mathbf{C}^T)^{-1}$$

establishing (13). Matrix  $\mathbf{C} \in \mathcal{C}_{pn}$  is full rank since it selects  $p$  distinct nodes, then  $\mathbf{C}(\mathbf{R}_x + \mathbf{R}_w)\mathbf{C}^T$  has rank  $p$  and thus it is invertible [33]. Substituting (13) into (15), yields (14).  $\square$

Indeed, Proposition 2 confirms that the optimal selection matrix  $\mathbf{C}^*$  is obtained solving problem (14) which, after leveraging the expression in (13), only requires knowledge of the given matrices  $\mathbf{H}$ ,  $\mathbf{R}_x$  and  $\mathbf{R}_w$ . The optimal sketch is then found substituting  $\mathbf{C}^*$  into (13) as  $\mathbf{H}_s^* = \mathbf{H}_s^*(\mathbf{C}^*)$ , a step incurring  $O(mnp + p^3)$  complexity. Naturally, this two-step solution procedure resulting in  $\{\mathbf{C}^*, \mathbf{H}_s^*(\mathbf{C}^*)\}$  entails no loss of optimality [34, Section 4.1.3].

Furthermore, the next proposition shows that problem (14), which yields the optimal  $\mathbf{C}^*$ , is equivalent to a binary optimization problem with a linear objective function and subject to linear matrix inequality (LMI) constraints.

**Proposition 3.** *Let  $\mathbf{c} \in \{0, 1\}^n$  be the binary vector that contains the diagonal elements of  $\mathbf{C}^T\mathbf{C}$ , i.e.  $\mathbf{C}^T\mathbf{C} = \text{diag}(\mathbf{c})$ .*

Then, in the context of Proposition 2, the optimization problem (14) over  $\mathbf{C}$  is equivalent to

$$\begin{aligned} & \min_{\substack{\mathbf{c} \in \{0,1\}^n, \\ \mathbf{Y}, \bar{\mathbf{C}}_\alpha}} \text{tr}[\mathbf{Y}] & (16) \\ & \text{s. t. } \bar{\mathbf{C}}_\alpha = \alpha^{-1} \text{diag}(\mathbf{c}), \quad \mathbf{c}^T \mathbf{1}_n = p \\ & \quad \begin{bmatrix} \mathbf{Y} - \mathbf{R}_y + \mathbf{H}\mathbf{R}_x \bar{\mathbf{C}}_\alpha \mathbf{R}_x \mathbf{H}^T & \mathbf{H}\mathbf{R}_x \bar{\mathbf{C}}_\alpha \\ \bar{\mathbf{C}}_\alpha \mathbf{R}_x \mathbf{H}^T & \bar{\mathbf{R}}_\alpha^{-1} + \bar{\mathbf{C}}_\alpha \end{bmatrix} \succeq \mathbf{0} \end{aligned}$$

where  $\bar{\mathbf{R}}_\alpha = (\mathbf{R}_x + \mathbf{R}_w - \alpha \mathbf{I}_n)$ ,  $\bar{\mathbf{C}}_\alpha$  and  $\mathbf{Y} \in \mathbb{R}^{m \times m}$  are auxiliary variables and  $\alpha > 0$  is any scalar satisfying  $\bar{\mathbf{R}}_\alpha \succ \mathbf{0}$ .

*Proof.* The inverse in the objective of (14) can be written as [17]

$$\begin{aligned} (\mathbf{C}(\mathbf{R}_x + \mathbf{R}_w)\mathbf{C}^T)^{-1} &= (\alpha \mathbf{I}_p - \alpha \mathbf{I}_p + \mathbf{C}(\mathbf{R}_x + \mathbf{R}_w)\mathbf{C}^T)^{-1} \\ &= \alpha^{-1} \mathbf{I}_p - \alpha^{-2} \mathbf{C}(\bar{\mathbf{R}}_\alpha^{-1} + \alpha^{-1} \mathbf{C}^T \mathbf{C})^{-1} \mathbf{C}^T, \end{aligned} \quad (17)$$

where  $\alpha \neq 0$  is a rescaling parameter, and in obtaining the second equality we used the Woodbury Matrix Identity [30]. Note that  $\alpha$  has to be such that  $\bar{\mathbf{R}}_\alpha = (\mathbf{R}_x + \mathbf{R}_w - \alpha \mathbf{I}_n)$  is still invertible. Substituting (17) into (14) and recalling that  $\mathbf{C}^T \mathbf{C} = \text{diag}(\mathbf{c})$ , we have that

$$\begin{aligned} & \min_{\substack{\mathbf{c} \in \{0,1\}^n, \bar{\mathbf{C}}_\alpha}} \text{tr} \left[ \mathbf{R}_y - \mathbf{H}\mathbf{R}_x \bar{\mathbf{C}}_\alpha \mathbf{R}_x \mathbf{H}^T \right. & (18) \\ & \quad \left. + \mathbf{H}\mathbf{R}_x \bar{\mathbf{C}}_\alpha (\bar{\mathbf{R}}_\alpha^{-1} + \bar{\mathbf{C}}_\alpha)^{-1} \bar{\mathbf{C}}_\alpha \mathbf{R}_x \mathbf{H}^T \right] \\ & \text{s. t. } \bar{\mathbf{C}}_\alpha = \alpha^{-1} \text{diag}(\mathbf{c}), \quad \mathbf{c}^T \mathbf{1}_n = p. \end{aligned}$$

Note that in (18) we optimize over a binary vector  $\mathbf{c} \in \mathbb{R}^n$  with exactly  $p$  nonzero entries, instead of a binary matrix  $\mathbf{C} \in \mathcal{C}_{pn}$ . The  $p$  nonzero elements in  $\mathbf{c}$  indicate the nodes to be sampled. Problem (18) can be reformulated as

$$\begin{aligned} & \min_{\substack{\mathbf{c} \in \{0,1\}^n, \\ \mathbf{Y}, \bar{\mathbf{C}}_\alpha}} \text{tr}[\mathbf{Y}] & (19) \\ & \text{s. t. } \mathbf{R}_y - \mathbf{H}\mathbf{R}_x \bar{\mathbf{C}}_\alpha \mathbf{R}_x \mathbf{H}^T \\ & \quad + \mathbf{H}\mathbf{R}_x \bar{\mathbf{C}}_\alpha (\bar{\mathbf{R}}_\alpha^{-1} + \bar{\mathbf{C}}_\alpha)^{-1} \bar{\mathbf{C}}_\alpha \mathbf{R}_x \mathbf{H}^T \preceq \mathbf{Y} \\ & \quad \bar{\mathbf{C}}_\alpha = \alpha^{-1} \text{diag}(\mathbf{c}), \quad \mathbf{c}^T \mathbf{1}_n = p \end{aligned}$$

where  $\mathbf{Y} \in \mathbb{R}^{m \times m}$ ,  $\mathbf{Y} \succeq \mathbf{0}$  is an auxiliary optimization variable. Using the Schur-complement lemma for positive definite matrices [34], problem (19) can be written as (16). Hence, to complete the proof we need to show that  $\bar{\mathbf{R}}_\alpha^{-1} + \bar{\mathbf{C}}_\alpha \succeq \mathbf{0}$  so that the aforementioned lemma can be invoked. To that end, suppose first that  $\alpha < 0$ . Then we have that  $\bar{\mathbf{R}}_\alpha \succ \mathbf{0}$  and  $\bar{\mathbf{C}}_\alpha = \alpha^{-1} \text{diag}(\mathbf{c}) \preceq \mathbf{0}$ , so that  $\bar{\mathbf{R}}_\alpha^{-1} + \bar{\mathbf{C}}_\alpha \succeq \mathbf{0}$  may not be positive definite. Suppose now that  $\alpha > 0$ . Then  $\bar{\mathbf{C}}_\alpha \succeq \mathbf{0}$  and there always exists a sufficiently small positive  $\alpha$  such that  $\bar{\mathbf{R}}_\alpha \succ \mathbf{0}$  since  $\mathbf{R}_w \succ \mathbf{0}$ . This implies that if  $\alpha$  is chosen such that  $\alpha > 0$  and  $\bar{\mathbf{R}}_\alpha = \mathbf{R}_x + \mathbf{R}_w - \alpha \mathbf{I}_n \succ \mathbf{0}$  (which are the conditions stated in the proposition), then  $\bar{\mathbf{R}}_\alpha^{-1} + \bar{\mathbf{C}}_\alpha$  is positive definite and problems (18) and (16) are equivalent.  $\square$

Problem (16) is an SDP optimization modulo the binary constraints on vector  $\mathbf{c}$ , which can be relaxed to yield a convex optimization problem (see Remark 3 for comments on the value of  $\alpha$ ). Once the relaxed problem is solved, the solution can be binarized again and matrix  $\mathbf{C}$  obtained from it. This procedure is detailed in Section V.

**Remark 3 (Numerical considerations).** While there always exists  $\alpha > 0$  such that  $\bar{\mathbf{R}}_\alpha = (\mathbf{R}_x + \mathbf{R}_w + \alpha \mathbf{I})$  is invertible, this value of  $\alpha$  has to be smaller than the smallest eigenvalue of  $\mathbf{R}_x + \mathbf{R}_w$ . In low-noise scenarios this worsens the condition number of  $\bar{\mathbf{R}}_\alpha$ , creating numerical instabilities when inverting said matrix (especially for large graphs). Alternative heuristic solutions to problems (14) and (16) are provided in Section V.

### B. Sampling the linear transform

As explained in Section II-A3, there may be setups where designing the new operator  $\mathbf{H}_s$  in (13), whose entries do not resemble those in  $\mathbf{H}$ , is costly or even infeasible. An alternative to bypass this problem consists in forming the sketch by taking  $p$  columns of  $\mathbf{H}$ , i.e., setting  $\mathbf{H}_s = \mathbf{H}\mathbf{C}^T$ . Although from an MSE performance point of view such a sketching design is suboptimal [cf. (13)], numerical tests carried out in Section VI suggest it can sometimes yield competitive performance. The optimal sampling strategy for sketches within this class is given in the following proposition.

**Proposition 4.** Let  $\mathbf{H}_s = \mathbf{H}\mathbf{C}^T$  be constructed from a subset of  $p$  columns of  $\mathbf{H}$ . Then, the optimal sampling matrix  $\mathbf{C}^*$  can be recovered from the diagonal elements  $\mathbf{c}^*$  of  $(\mathbf{C}^*)^T \mathbf{C}^* = \text{diag}(\mathbf{c}^*)$ , where  $\mathbf{c}^*$  is the solution to the following problem

$$\begin{aligned} & \min_{\substack{\mathbf{c} \in \{0,1\}^n, \\ \mathbf{Y}, \bar{\mathbf{C}}}} \text{tr}[\mathbf{Y}] & (20) \\ & \text{s. t. } \bar{\mathbf{C}} = \text{diag}(\mathbf{c}), \quad \mathbf{c}^T \mathbf{1}_n = p \end{aligned}$$

$$\begin{bmatrix} \mathbf{Y} - \mathbf{R}_y + 2\mathbf{H}\bar{\mathbf{C}}\mathbf{R}_x\mathbf{H}^T & \mathbf{H}\bar{\mathbf{C}} \\ \bar{\mathbf{C}}\mathbf{H}^T & (\mathbf{R}_x + \mathbf{R}_w)^{-1} \end{bmatrix} \succeq \mathbf{0}.$$

*Proof.* Defining matrix  $\bar{\mathbf{C}} = \text{diag}(\mathbf{c})$ , the estimated output is

$$\hat{\mathbf{y}} = \mathbf{H}\mathbf{C}^T \mathbf{C}(\mathbf{x} + \mathbf{w}) = \mathbf{H}\text{diag}(\mathbf{c})(\mathbf{x} + \mathbf{w}) = \mathbf{H}\bar{\mathbf{C}}(\mathbf{x} + \mathbf{w}).$$

Since the desired output is  $\mathbf{y} = \mathbf{H}\mathbf{x}$ , the MSE simplifies to

$$\begin{aligned} & \mathbb{E} [\|\mathbf{H}\mathbf{x} - \mathbf{H}\bar{\mathbf{C}}(\mathbf{x} + \mathbf{w})\|_2^2] & (21) \\ & = \text{tr} [\mathbf{H}\mathbf{R}_x \mathbf{H}^T - 2\mathbf{H}\bar{\mathbf{C}}\mathbf{R}_x \mathbf{H}^T + \mathbf{H}\bar{\mathbf{C}}(\mathbf{R}_x + \mathbf{R}_w)\bar{\mathbf{C}}\mathbf{H}^T]. \end{aligned}$$

Introducing the auxiliary variable  $\mathbf{Y} \in \mathbb{R}^{m \times m}$ ,  $\mathbf{Y} \succeq \mathbf{0}$ , minimizing (21) with  $\mathbf{C} \in \mathcal{C}_{pn}$  is equivalent to solving

$$\begin{aligned} & \min_{\substack{\mathbf{c} \in \{0,1\}^n, \\ \mathbf{Y}, \bar{\mathbf{C}}}} \text{tr}[\mathbf{Y}] & (22) \\ & \text{s. t. } \bar{\mathbf{C}} = \text{diag}(\mathbf{c}), \quad \mathbf{c}^T \mathbf{1}_n = p \\ & \quad \mathbf{R}_y - 2\mathbf{H}\bar{\mathbf{C}}\mathbf{R}_x \mathbf{H}^T + \mathbf{H}\bar{\mathbf{C}}(\mathbf{R}_x + \mathbf{R}_w)\bar{\mathbf{C}}\mathbf{H}^T \preceq \mathbf{Y}. \end{aligned}$$

Finally, using the Schur complement-based lemma for positive semidefiniteness [34], then (22) can be shown equivalent to (20), completing the proof.  $\square$

## IV. INVERSE SKETCHING PROBLEM

This section presents the optimal sampling  $\mathbf{C}^* \in \mathcal{C}_{np}$  and sketching  $\mathbf{H}_s^* \in \mathbb{R}^{m \times p}$  solutions for the inverse problem in Fig. 2 and Section II-A2. Paralleling the structure of the previous section, we first analyze the particular case where the observations are noise free, then shift to the general noisy case, and finally look at a suboptimal scheme where the sketch is formed by taking rows of the linear transformation  $\mathbf{H}^T$ .

Since proof arguments are similar to those used for the direct sketching problem, we skip the details that can be found in [2].

In the absence of noise corrupting the output observations, then (8) simplifies to

$$\min_{\mathbf{C} \in \mathcal{C}_{n,p}, \mathbf{H}_s} \mathbb{E} [\|\mathbf{H}^T(\mathbf{H}_s \mathbf{C} \mathbf{x}) - \mathbf{x}\|_2^2]. \quad (23)$$

Assuming that  $\mathbf{H}$  is full rank – so that matrix  $\mathbf{A}_{\text{LS}} = (\mathbf{H}\mathbf{H}^T)^{-1}\mathbf{H}$  in (7) exists –, the optimal  $\mathbf{C}^*$  and  $\mathbf{H}_s^*$  solving (23) are characterized in the following proposition, which shows that once more perfect reconstruction is possible.

**Proposition 5.** *Let  $\mathbf{x} \in \mathbb{R}^n$  be a  $k$ -bandlimited signal with known spectral template  $\mathbf{T} \in \mathbb{C}^{k \times k}$  and let  $\mathbf{H} \in \mathbb{R}^{m \times n}$  be a linear transformation. Let  $\mathbf{H}_s \in \mathbb{R}^{m \times p}$  be a reduced-input dimensionality sketch,  $p \leq n$  and  $\mathbf{C} \in \mathcal{C}_{pn}$  be a selection matrix. If  $p = k$ , a sampling  $\mathbf{C}^*$  designed such that  $\text{rank}\{\mathbf{C}^* \mathbf{V}_k\} = p = k$  is optimal for (23). Moreover,  $\hat{\mathbf{y}} = \mathbf{H}_s^* \mathbf{C}^* \mathbf{x}$  yields the LS estimate  $\hat{\mathbf{y}}_{\text{LS}} = \mathbf{A}_{\text{LS}} \mathbf{x} = (\mathbf{H}\mathbf{H}^T)^{-1} \mathbf{H} \mathbf{x}$  provided that the optimum  $\mathbf{H}_s^*$  is given by*

$$\mathbf{H}_s^*(\mathbf{C}^*) = \mathbf{A}_{\text{LS}} \mathbf{V}_k (\mathbf{C}^* \mathbf{V}_k)^{-1}. \quad (24)$$

In this noise-free case, the result of Proposition 5 is identical to that of Proposition 1 with a direct transform  $\mathbf{H} = \mathbf{A}_{\text{LS}}$ . This is consistent with the fact that in the present setting,  $\mathbf{H}_s$  is a sketch of the inverse mapping relating outputs to inputs.

#### A. Noisy case

As in Section III-A we consider that the noise  $\mathbf{w} \in \mathbb{R}^n$  is independent of  $\mathbf{x}$ , has zero mean and that its covariance matrix satisfies  $\mathbf{R}_w \succ \mathbf{0}$ . Upon defining  $\mathbf{G} = \mathbf{H}^T \mathbf{A}_{\text{LS}}$ , the next proposition characterizes the optimal  $\mathbf{C}^*$  and  $\mathbf{H}_s^*$  matrices.

**Proposition 6.** *If  $\mathbf{H}$  is full rank, the solution to problem (8) is given by  $\mathbf{C}^*$  and  $\mathbf{H}_s^* = \mathbf{H}_s^*(\mathbf{C}^*)$ , where*

$$\mathbf{H}_s^*(\mathbf{C}) = \mathbf{A}_{\text{LS}} \mathbf{R}_x \mathbf{C}^T (\mathbf{C}(\mathbf{R}_x + \mathbf{R}_w) \mathbf{C}^T)^{-1}. \quad (25)$$

The optimum selection matrix  $\mathbf{C}^*$  is obtained from solving

$$\min_{\mathbf{C} \in \mathcal{C}_{n,p}} \text{tr} [\mathbf{R}_x - \mathbf{G} \mathbf{R}_x \mathbf{C}^T (\mathbf{C}(\mathbf{R}_x + \mathbf{R}_w) \mathbf{C}^T)^{-1} \mathbf{C} \mathbf{R}_x \mathbf{G}^T]. \quad (26)$$

As was the case for the direct problem, the joint design of the optimal selection matrix  $\mathbf{C}^*$  and the optimal sketch  $\mathbf{H}_s^*$  can be carried out as a two-step process. First  $\mathbf{C}^*$  is found as the solution to (26), which only requires as input  $\mathbf{R}_x$ ,  $\mathbf{G}$  and  $\mathbf{R}_w$ . Then, the optimal sketch is found using (25)  $\mathbf{H}_s^* = \mathbf{H}_s^*(\mathbf{C}^*)$ .

Moreover, note that the optimal sketch  $\mathbf{H}_s^*$  is tantamount to the LS operator  $\mathbf{A}_{\text{LS}} = (\mathbf{H}\mathbf{H}^T)^{-1} \mathbf{H}$  acting on a preprocessed version of  $\mathbf{x}$ , via the matrix  $\mathbf{R}_x \mathbf{C}^T (\mathbf{C}(\mathbf{R}_x + \mathbf{R}_w) \mathbf{C}^T)^{-1}$ . What this preprocessing entails is, essentially, choosing the samples of  $\mathbf{x}$  with the optimal tradeoff between the signal in the multiplicative term  $\mathbf{R}_x \mathbf{C}^T$  and the noise in the inverse term  $(\mathbf{C}(\mathbf{R}_x + \mathbf{R}_w) \mathbf{C}^T)^{-1}$ . Also observe that, while computation of the inverse-mapping sketch  $\mathbf{H}_s^*$  involves the (costly) computation of  $(\mathbf{H}\mathbf{H}^T)^{-1}$ , this is carried out entirely off line.

Finally, the optimization problem (26) over  $\mathbf{C}$  is equivalent to a problem reminiscent of an SDP save the binary constraints, as shown next.

**Proposition 7.** *In the setting of Proposition 6, the optimum selection matrix  $\mathbf{C}^*$  is such that the diagonal elements  $\mathbf{c}^*$  of  $(\mathbf{C}^*)^T \mathbf{C}^* = \text{diag}(\mathbf{c}^*)$ , are given by the solution to the problem*

$$\min_{\substack{\mathbf{c} \in \{0,1\}^n, \\ \mathbf{Y}, \bar{\mathbf{C}}_\alpha}} \text{tr}[\mathbf{Y}] \quad (27)$$

$$\text{s. t. } \bar{\mathbf{C}}_\alpha = \alpha^{-1} \text{diag}(\mathbf{c}), \quad \mathbf{c}^T \mathbf{1}_n = p$$

$$\begin{bmatrix} \mathbf{Y} - \mathbf{R}_x + \mathbf{G} \mathbf{R}_x \bar{\mathbf{C}}_\alpha \mathbf{R}_x \mathbf{G}^T & \mathbf{G} \mathbf{R}_x \bar{\mathbf{C}}_\alpha \\ \bar{\mathbf{C}}_\alpha \mathbf{R}_x \mathbf{G}^T & \bar{\mathbf{R}}_\alpha^{-1} + \bar{\mathbf{C}}_\alpha \end{bmatrix} \succeq \mathbf{0},$$

where  $\bar{\mathbf{R}}_\alpha = (\mathbf{R}_x + \mathbf{R}_w - \alpha \mathbf{I}_n)$ ,  $\bar{\mathbf{C}}_\alpha$  and  $\mathbf{Y} \in \mathbb{R}^{n \times n}$  are auxiliary variables and  $\alpha > 0$  is any scalar satisfying  $\bar{\mathbf{R}}_\alpha \succ \mathbf{0}$ .

#### B. Sampling the linear transformation

Here we look at setups where the sketch  $\mathbf{H}_s$  is constrained to be a submatrix of  $\mathbf{H}$ . In the context of linear inverse problems, this amounts to saying that  $\mathbf{H}_s = \mathbf{H} \mathbf{C}^T$  is formed using  $p$  columns of  $\mathbf{H}$ . With  $\bar{\mathbf{H}} = \mathbf{H}^T \mathbf{H}$  denoting the  $n \times n$  Gram matrix of  $\mathbf{H}$ , the solution to (8) for sketches of the form  $\mathbf{H}_s = \mathbf{H} \mathbf{C}^T$  is given by the following proposition.

**Proposition 8.** *Let  $\mathbf{H}_s = \mathbf{H} \mathbf{C}^T$  be constructed from a subset of  $p$  columns of  $\mathbf{H}$ . Then, the optimal sampling matrix  $\mathbf{C}^*$  can be recovered from vector  $\mathbf{c}^*$  that contains the diagonal elements of  $(\mathbf{C}^*)^T \mathbf{C}^* = \text{diag}(\mathbf{c}^*)$ , where  $\mathbf{c}^*$  is the solution to the following problem*

$$\min_{\substack{\mathbf{c} \in \{0,1\}^n, \\ \mathbf{Y}, \bar{\mathbf{C}}}} \text{tr}[\mathbf{Y}] \quad (28)$$

$$\text{s. t. } \bar{\mathbf{C}} = \text{diag}(\mathbf{c}), \quad \mathbf{c}^T \mathbf{1}_n = p$$

$$\begin{bmatrix} \mathbf{Y} - \mathbf{R}_x + 2\bar{\mathbf{H}}\bar{\mathbf{C}}\mathbf{R}_x & \bar{\mathbf{H}}\bar{\mathbf{C}} \\ \bar{\mathbf{C}}\bar{\mathbf{H}} & (\mathbf{R}_x + \mathbf{R}_w)^{-1} \end{bmatrix} \succeq \mathbf{0}.$$

## V. HEURISTIC APPROACHES

In this section, several heuristics are outlined for tackling the linear sketching problems described so far. The rationale is that oftentimes the problems posed in Sections III and IV can be intractable, ill-conditioned, or, just too computationally expensive even if carried out off line. In fact, the optimal solution  $\mathbf{C}^*$  to (14) or (26) can be obtained by evaluating the objective function in each one of the  $\binom{n}{p}$  possible solutions. Table I lists the complexity of each of the proposed methods. Additionally, the time (in seconds) taken to run the simulation related to Fig. 6 is also included in the table for comparison. In all cases, after obtaining  $\mathbf{C}^*$ , forming the optimal value of  $\mathbf{H}_s^*$  entails  $O(mnp + p^3)$  operations, see (13) and (25).

#### A. Convex relaxation (SDP)

Recall that the main difficulty when solving (16), (20), (27) and (28) are the *binary* constraints that render the problems non-convex and, in fact, NP-hard. A standard alternative to overcome this difficulty is to relax the binary constraint  $\mathbf{c} \in \{0,1\}^n$  on the sampling vector as  $\mathbf{c} \in [0,1]^n$ . This way, the optimization problems become convex and can be solved with polynomial complexity in  $O((m+n)^{3.5})$  operations as per the SDP formulations in (16) and (27) [34].

Once a solution to the relaxed problem is obtained, two ways of recovering a binary vector  $\mathbf{c}$  are considered. The

Method	Number of operations	Time [s]
Optimal solution	$O\left(\binom{n}{p}\right)$	$> 10^6$
Convex relaxation (SDP)	$O((m+n)^{3.5})$	25.29
Noise-blind heuristic	$O(n \log n + nm)$	0.46
Noise-aware heuristic	$O(n^3 + nm)$	21.88
Greedy approach	$O(mn^2p^2 + np^4)$	174.38

Table I: Computational complexity of the heuristic methods proposed in Section V to solve optimization problems in Sections III and IV: (i) Number of operations required; (ii) Time (in seconds) required to solve the problem in Sec. VI-D, see Fig. 6. Also, for the sake of comparison, we have included a row containing the cost of the optimal solution, meaning the cost of solving the optimization problems exactly with no relaxation on the binary constraints.

first one is a deterministic method referred to as thresholding (SDP-Threshold.), which simply consists in setting the largest  $p$  elements to 1 and the rest to 0. The second one consists in computing  $\mathbf{p}_c = \mathbf{c}/\|\mathbf{c}\|_1$ , which can be viewed as a probability distribution over the nodes (SDP-Random). The sampled nodes are then drawn at random from this distribution, see [35]. This should be done once, off line, and the same selection matrix used for every incoming input (or output). Although not pursued here, also pertinent are formulations that penalize the objective with  $\|\mathbf{c}\|_1$  and leverage  $\ell_1$ -norm minimization advances to promote sparsity on  $\mathbf{c}$ .

### B. Noise-aware heuristic (NAH)

An heuristic that is less computationally costly than the SDP in Section V-A can be obtained as follows. Consider for instance the objective function of the direct problem (14)

$$\text{tr} \left[ \mathbf{R}_y - \mathbf{H} \mathbf{R}_x \mathbf{C}^T (\mathbf{C}(\mathbf{R}_x + \mathbf{R}_w) \mathbf{C}^T)^{-1} \mathbf{C} \mathbf{R}_x \mathbf{H}^T \right], \quad (29)$$

where we note that the noise imposes a trade-off in the selection of samples. More precisely, while some nodes are very important in contributing to the transformed signal, as determined by the rows of  $\mathbf{R}_x \mathbf{H}^T$ , those same nodes might provide very noisy measurements, as determined by the corresponding submatrix of  $(\mathbf{R}_x + \mathbf{R}_w)$ . Taking this trade-off into account, the proposed noise-aware heuristic (NAH) consists of selecting the rows of  $(\mathbf{R}_x + \mathbf{R}_w)^{-1/2} \mathbf{R}_x \mathbf{H}^T$  with highest  $\ell_2$  norm. This polynomial-time heuristic entails  $O(n^3)$  operations to compute the inverse square root of  $(\mathbf{R}_x + \mathbf{R}_w)$  [36] and  $O(mn)$  to compute its multiplication with  $\mathbf{R}_x \mathbf{H}^T$  as well as the norm. Note that  $(\mathbf{R}_x + \mathbf{R}_w)^{-1/2} \mathbf{R}_x \mathbf{H}^T$  resembles a signal-to-noise ratio (SNR), and thus the noise-aware heuristic proposed is attempting to maximize this measure of SNR.

### C. Noise-blind heuristic (NBH)

Another heuristic that incurs an even lower computational cost can also be obtained by inspection of (29). Recall that the complexity of the NAH is dominated by the computation of  $(\mathbf{R}_x + \mathbf{R}_w)^{-1/2}$ . An even faster heuristic solution can thus be obtained by simply ignoring this term, which accounted

for the noise present in the chosen samples. Accordingly, in what we termed the noise-blind heuristic (NBH) we simply select the  $p$  rows of  $\mathbf{R}_x \mathbf{H}^T$  that have maximum  $\ell_2$  norm. The resulting NBH is straightforward to implement, entails  $O(mn)$  operations for computing the norm of  $\mathbf{R}_x \mathbf{H}^T$  and  $O(n \log n)$  operations for the sorting algorithm [37]. It is shown in Section VI to yield satisfactory performance, especially if the noise variance is low or the linear transform has favorable structure. In summary, the term noise-blind stems from the fact that we are selecting the nodes that yield the highest output energy as measured by  $\mathbf{R}_x \mathbf{H}^T$ , while being completely agnostic to the noise corrupting the samples in those nodes.

The analysis of both the NAH (Section V-B) and NBH (Section V-C) can be readily extended to the linear inverse problem by inspecting the objective function in (26).

### D. Greedy approach

Another alternative to approximate the solution of (14) and (26), or approximate the solution of minimizing (21) (and its inverse problem counterpart) over  $\mathcal{C}_{np}$ , is to implement an iterative greedy algorithm that adds nodes to the sampling set incrementally. At each iteration, the node that reduces the MSE the most is incorporated to the sampling set. Considering problem (14) as an example, first, one-by-one all  $n$  nodes are tested and the one that yields the lowest value of the objective function in (14) is added to the sampling set. Then, the sampling set is augmented with one more node by choosing the one that yields the lowest optimal objective among the remaining  $n - 1$  nodes. The procedure is repeated until  $p$  nodes are selected in the sampling set. This way only  $n + (n-1) + \dots + (n-(p-1)) < np$  evaluations of the objective function (14) are required. Note that each evaluation of (14) entails  $O(mnp + p^3)$  operations, so that the overall cost of the greedy approach is  $O(mn^2p^2 + np^4)$ . Greedy algorithms have well-documented merits for sample selection, even for non-submodular objectives like the one in (14); see [18], [38].

## VI. NUMERICAL TESTS

To demonstrate the effectiveness of the sketching methods developed in this paper, four numerical test cases are considered. In Sec. VI-A and VI-B we look at the case where the transformation to approximate is a GFT and the signals are bandlimited. In Sec. VI-A we assume that we do not have access to the GFT coefficients and formulate this as an inverse problem. In Sec. VI-B we assume that the GFT is known and address the design as a direct problem. Then, in Sec. VI-C we consider an (inverse) linear estimation problem in a wireless sensor network. The transform to approximate is the (fat) linear estimator and choosing samples in this case boils down to selecting the sensors acquiring the measurements [17, Sec. VI-A]. Finally, in Sec. VI-D, we look at the classification of digits from the MNIST Handwritten Digit database [39]. The linear approximation to sketch in this case is the combination of a linear support vector machine (SVM) classifier and a Principal Component Analysis (PCA) transform and our goal is to run the classification by processing only a few (optimally selected) pixels without having to explicitly obtain the PCA coefficients.

Throughout, we quantify the error performance of the sketching-as-sampling technique presented in this paper (implemented by each of the five heuristics introduced) and compare it to that of existing alternatives. More specifically, we consider:

- a) The sketching plus sampling algorithms proposed in this paper, namely: a1) the random sampling scheme based on the convex relaxation (SDP-Random, Sec. V-A); a2) the thresholding sampling scheme based on the convex relaxation (SDP-Threshold, Sec. V-A); a3) the noise-aware heuristic (NAH, Sec. V-B); a4) the noise-blind heuristic (NBH, Sec. V-C); and a5) the greedy approach (Sec. V-D).
- b) Algorithms for sampling bandlimited graph signals, namely: b1) the experimental design sampling (EDS) method proposed in [40]; and b2) the spectral proxies (SP) greedy-based method proposed in [15, Algorithm 1]. Recalling that the columns of  $\mathbf{V}$  represent the frequencies of the graph (cf. Sec. II), the scheme in [40] uses the weights  $\kappa_j = \sup_{1 \leq i \leq n} |\sqrt{n} \mathbf{V}_{j,i}|$  to construct a probability distribution over the nodes and then sample with replacement according to this distribution. Since this is equivalent to defining  $\kappa_j$  as the  $\ell_\infty$  norm of the rows of  $\mathbf{V}$ , we also test  $\ell_2$  norm of the rows (which corresponds to the method proposed in [35]) and the row-wise  $\ell_1$  norms. These methods are denoted as EDS-1, EDS-2 and EDS- $\infty$  when the value of  $\kappa_j$  is obtained by the  $\ell_1$ ,  $\ell_2$  and  $\ell_\infty$  norms of the rows of  $\mathbf{V}$ , respectively.
- c) Traditional sketching algorithms, namely Algorithms 2.4, 2.6 and 2.11 described in (the tutorial paper) [11], and respectively denoted in the figures as Sketching 2.4, Sketching 2.6 and Sketching 2.11. Note that these schemes can only be used for the inverse problem, hence they will be tested only in Secs. VI-A and VI-C.

For the sampling algorithms in a) and b), the matrix  $\mathbf{H}_s^*(\mathbf{C})$  is obtained using the optimal expression in (13) and (25), evaluated on the corresponding obtained value for  $\mathbf{C}$ . Differently, when using the traditional sketching methods in c), the algorithms in [11] do not compute a selection matrix  $\mathbf{C}$  but rather a sketch  $\mathbf{K}$  that is applied to both the incoming signal and the linear transform (see Sec. II-B and [11] for further details). Finally, one must note that the sketching schemes in c), the EDS schemes in b1) and the scheme described in a1) are random. All other schemes, i.e., all but one of the algorithms in a) and the SP method in b2), are deterministic.

To aid readability and reduce the number of curves on the figures presented next, only the best-performing among the three EDS methods in b1) is shown. A similar strategy is implemented for the three sketching algorithms in c).

#### A. Approximating the GFT as an inverse problem

Obtaining alternative data representations that would offer better insights and facilitate the resolution of specific tasks is one of the main concerns in signal processing and machine learning. In the context of GSP, the GFT decomposes graph signals into different modes of signal variation with respect to the underlying network topology. In the particular case of a directed cycle graph, the GFT reduces to the DFT, or, when considering stationary random signals as supported on a

graph described by their covariance matrix, the GFT amounts to computing the PCA coefficients. Therefore, computing the GFT of a signal is a relevant concern of GSP [6].

The relationship between a graph signal  $\mathbf{x}$  and its GFT  $\tilde{\mathbf{x}}_k$  is given by a linear operation, namely projecting the signal onto the subspace spanned by the  $k$  eigenvectors of the graph shift operator  $\mathbf{S}$  contained in  $\mathbf{V}_k$ . Hence, the task of obtaining GFT coefficients falls under the scope of the sketching-as-sampling method presented in this paper. More precisely, we have a  $k$ -bandlimited input signal  $\mathbf{x}$  and want to compute an output signal  $\mathbf{y} = \tilde{\mathbf{x}}_k = \mathbf{V}_k^H \mathbf{x}$  that contains the nonzero GFT coefficients  $\tilde{\mathbf{x}}_k$ . This is an instance of the direct problem. Alternatively, we can understand  $\mathbf{x}$  as being synthesized by the columns of  $\mathbf{V}_k$ , i.e.,  $\mathbf{x} = \mathbf{V}_k \tilde{\mathbf{x}}_k$ . Now the (known) output is  $\mathbf{x}$  and the (unknown) input to be estimated is  $\tilde{\mathbf{x}}_k$ . The latter falls under the context of linear inverse problems. Here we consider computing the GFT as an inverse problem, and in the following Sec. VI-B we study it as a direct problem.

In what follows, we set the graph shift operator  $\mathbf{S}$  to be the adjacency matrix of the underlying undirected graph  $\mathcal{G}$ . Because the shift is symmetric, it can be decomposed as  $\mathbf{S} = \mathbf{V} \mathbf{\Lambda} \mathbf{V}^T$ . So the GFT to approximate is  $\mathbf{V}^T$ , a real orthonormal matrix that projects signals onto the eigenvector space of the adjacency of  $\mathcal{G}$ . With this notation in place, for this first experiment we assume to have access to 100 noisy realizations of this  $k$ -bandlimited graph signal  $\{\mathbf{x}_t + \mathbf{w}_t\}_{t=1}^{100}$ , where  $\mathbf{w}_t$  is zero-mean Gaussian noise with  $\mathbf{R}_w = \sigma_w^2 \mathbf{I}_n$ . The objective is to compute  $\{\tilde{\mathbf{x}}_{k,t}\}_{t=1}^{100}$ , that is, the  $k$  active GFT coefficients of each one of these graph signals. Since  $\mathbf{x} = \mathbf{V}_k \tilde{\mathbf{x}}_k$ , we can model this problem as an inverse problem, as in Sec. IV in which the linear transform is  $\mathbf{H}^T = \mathbf{V}_k$ , the measurable output is  $\mathbf{x}$ , and the input to be estimated is  $\mathbf{y} = \tilde{\mathbf{x}}_k$ , see Fig. 2. Then, instead of computing the GFT  $\tilde{\mathbf{x}}_k$  by processing all  $n$  nodes, we proceed to select  $p \geq k$  nodes,  $p \ll n$  and approximate the  $k$  GFT coefficients by applying the designed sketch  $\mathbf{H}_s^*$  to only these  $p$  nodes. This method then serves as a fast computation of the  $k$  GFT coefficients.

To run the algorithms, we consider two types of undirected graphs: a stochastic block model (SBM) and a small-world (SW) network. Let  $\mathcal{G}_{\text{SBM}}$  be denote a SBM network with  $n$  total nodes and  $c$  communities with  $n_b$  nodes in each community,  $b = 1, \dots, c$ ,  $\sum_{b=1}^c n_b = n$  [41]. The probability of drawing an edge between nodes within the same community is  $p_b$  and the probability of drawing an edge between any node in community  $b$  and any node in community  $b'$  is  $p_{bb'}$ . Similarly, let  $\mathcal{G}_{\text{SW}}$  be a SW network with  $n$  nodes described by parameters  $p_e$  (probability of drawing an edge between nodes) and  $p_r$  (probability of rewiring edges), see [42] for details. In the first experiment, we study signals  $\mathbf{x} \in \mathbb{R}^n$  supported on either the SBM or the SW networks. In each of the test cases presented,  $\mathcal{G} \in \{\mathcal{G}_{\text{SBM}}, \mathcal{G}_{\text{SW}}\}$  denotes the underlying graph, and  $\mathbf{A} \in \{0, 1\}^{n \times n}$  its associated adjacency matrix. The simulation parameters are set as follows. The number of nodes is  $n = 96$  and the bandwidth is  $k = 10$ . For the SBM, we set  $c = 4$  communities of  $n_b = 24$  nodes in each, with edge probabilities  $p_b = 0.8$  and  $p_{bb'} = 0.2$  for  $b \neq b'$ . For the SW case, we set the edge and rewiring probabilities as  $p_e = 0.2$  and  $p_r = 0.7$ . The goal is to approximate (estimate)

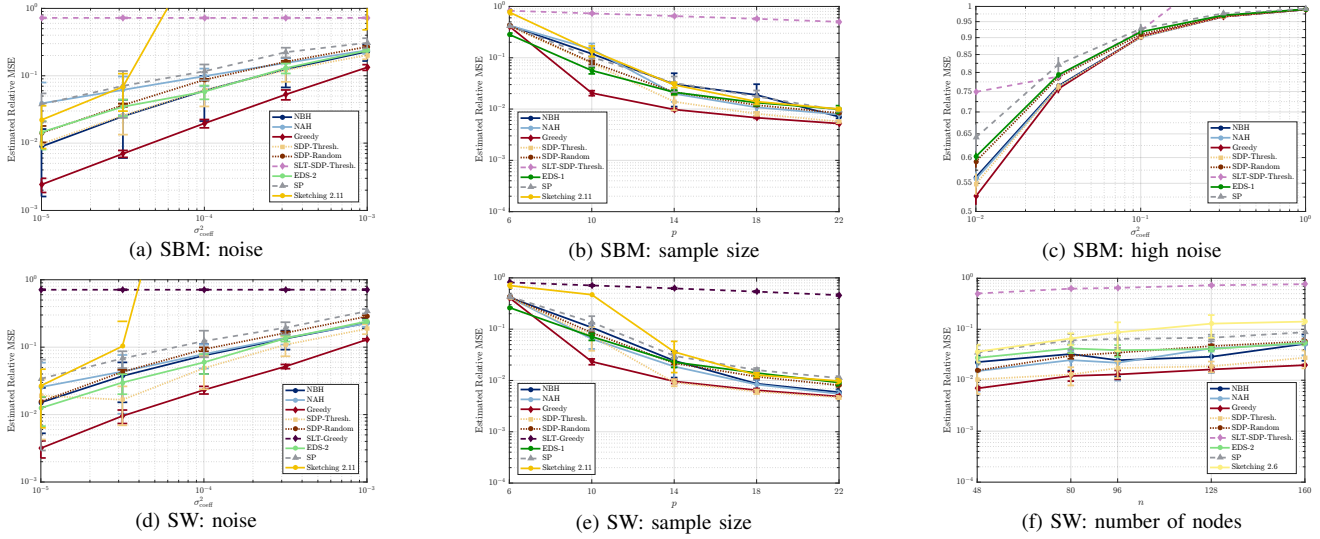


Figure 3. Approximating the GFT as an inverse sketching problem. Relative estimated MSE. Graph supports: SBM (top) and SW (bottom). Legends: SDP-Random (scheme in a1); SDP-Thresh. (scheme in a2); NAH (scheme in a3), NBH (scheme in a4); Greedy (scheme in a5); SLT, EDS-1, EDS-2 (schemes in b1), SP (scheme in b2); and Sketching 2.6, Sketching 2.11 (schemes in c).

the  $k$  GFT coefficients as  $\hat{\mathbf{y}} = \mathbf{H}_s^*(\mathbf{C})\mathbf{C}(\mathbf{x} + \mathbf{w})_s$ , where  $\mathbf{C}$  is designed according to the various methods under study, and with  $\mathbf{H}_s^*(\mathbf{C})$  given by (25). The metric to assess the reconstruction performance is the relative mean squared error (MSE) computed as  $\mathbb{E}[\|\hat{\mathbf{y}} - \tilde{\mathbf{x}}_k\|_2^2] / \mathbb{E}[\|\tilde{\mathbf{x}}_k\|_2^2]$ . We simulate 100 different sequences  $\{\mathbf{x}_t\}_{t=1}^{100}$  of 100 signals in each sequence, totaling 10,000 signals. We average the error on these noisy realizations to estimate the MSE. We repeat this simulation for 5 different random graph realizations. For the methods that use the covariance matrix  $\mathbf{R}_x$  as input, we estimate  $\mathbf{R}_x$  from 500 realizations of  $\mathbf{x}$ , which we regarded as training samples and are not used for estimating the relative MSE. Finally, for the methods in which the sampling method is random, we perform the node selection 10 different times and average the results.

For each of the graph types, we carry out two main simulations. In the first one, we consider the number of selected samples to be fixed to  $p = k = 10$  and consider different noise power levels  $\sigma_w^2 = \sigma_{\text{coeff}}^2 \cdot \mathbb{E}[\|\mathbf{x}\|_2^2]$  by varying  $\sigma_{\text{coeff}}^2$  from  $10^{-5}$  to  $10^3$  and where  $\mathbb{E}[\|\mathbf{x}\|_2^2]$  is estimated from the training samples. For the second simulation, we fix the noise to  $\sigma_{\text{coeff}}^2 = 10^{-4}$  and vary  $p$  from 6 to 22. After this, we run two more simulations, one in which we consider the SBM graph in high noise scenarios, where  $p = k$  is set to 10 and  $\sigma_{\text{coeff}}^2$  varies from  $10^{-2}$  to  $10^0$ ; and another one in which we consider the SW graph, set  $k = 10$ ,  $p = 12$ ,  $\sigma_{\text{coeff}}^2 = 10^{-4}$  and vary  $n$  from 48 to 160. The results of this experiment are summarized in the six plots shown in Fig. 3.

First, Figs. 3a and 3d show the estimated relative MSE as a function of  $\sigma_{\text{coeff}}^2$  for fixed  $p = k = 10$ . For graph signals supported on  $\mathcal{G}_{\text{SBM}}$  (Fig. 3a), we observe that the best performance is achieved by our greedy scheme a5) which, for low-noise scenarios, is one order of magnitude better than the EDS-2 scheme (which is the best one among all the ones in b1). In fact, all the methods in a) except for a1) perform better than the EDS-2 scheme. We also note that the performance of the SP scheme in b2) is similar (albeit slightly worse) to that of all the other schemes. Among the traditional

sketching methods in c), the Algorithm 2.11 is the one with the minimum error, but performs quite poorly compared to all other alternatives. Finally, we note that directly sampling the linear transform yields an almost constant performance, but considerably worse than that of the remaining methods. The performance analysis for graphs signals supported on  $\mathcal{G}_{\text{SW}}$  (Fig. 3d) is very similar, with the exception of the EDS-2 scheme outperforming the NBH, a4).

Second, the relative MSE as a function of  $p$  for fixed  $\sigma_{\text{coeff}}^2$  for the SBM and SW networks is plotted in Figs. 3b and 3e, respectively. For the SBM case, we observe that, again, the greedy approach outperforms all other methods, except for the degenerate case of  $p = 6 < k$ , when the EDS-1 scheme yields a better performance. We also note that our SDP method in a2) performs well, especially for  $p > k$ . Among the competing alternatives, the EDS-1 scheme in b1) exhibits the smallest error, although not too far from the SP method in b2) and the Algorithm 2.11 in c). For signals defined on  $\mathcal{G}_{\text{SW}}$  (Fig. 3e), our greedy approach in a5) still is the best, although for  $p > k$  its performance is matched by that of the SDP-Thresh. in a2). For  $p > k$ , the NAH in a3) as well as the NBH in a4) outperform the alternatives in b) and c). For large  $p$ , all methods have comparable performance in the order of  $10^{-2}$ .

Third, Fig. 3c shows the results for the SBM case with high-noise, where  $\sigma_{\text{coeff}}^2$  varies from  $10^{-2}$  to 1, and the number of samples is fixed to  $p = k = 10$ . Once again, we observe that the greedy approach in a5) achieves the best performance. We also note that all proposed schemes in a) outperform the existing methods. Performance is almost the same for the highest-noise scenario considered. The traditional sketching method is not shown for having a relative MSE worse than 1 across all values of  $\sigma_{\text{coeff}}^2$  considered.

Fourth and final, we set  $\sigma_{\text{coeff}}^2 = 10^{-4}$ ,  $p = k + 2 = 12$ , consider an SW graph and plot the recovery error as a function of the size of the graph  $n$ . The results, shown in Fig. 3f, reveal that the greedy approach in a5) has the best performance, with the SDP-Thresh. in a2) following closely. As before, the NBH

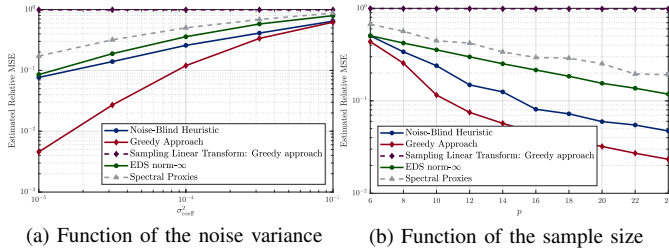


Figure 4. Approximating the GFT as a direct sketching problem for a large network. Relative estimated MSE  $\|\hat{\mathbf{y}} - \tilde{\mathbf{x}}_k\|^2 / \|\tilde{\mathbf{x}}_k\|^2$  for the problem of estimating the  $k = 10$  frequency components of a bandlimited graph signal from noisy observations, supported on an ER graph with  $p = 0.1$  and size  $n = 10,000$ . (a) As a function of  $\sigma_{\text{coeff}}^2$  for fixed  $p = k = 10$ . (b) As a function of the  $p$  for fixed  $\sigma_{\text{coeff}}^2 = 10^{-4}$ .

and NAH in a3) and a4) also outperform all the competing alternatives.

So, all in all, we have analyzed the performance of the proposed sketching-as-sampling method for different solutions, graph supports and parameter variations for small-sized graphs of around  $n = 100$  nodes. We have observed that in all cases the greedy approach (Sec. V-D) works best, and that the SDP-Threshold. (Sec. V-A) also has a very good performance. In almost all cases, these two methods outperform the competing alternatives. We also note that for  $p < k$ , the EDS graph signal sampling technique seems to work better.

### B. Approximating the GFT in a large scale network

Consider now the problem of approximating the  $k$  GFT coefficients as a direct sketching problem. Namely, we focus on  $\tilde{\mathbf{x}}_k = \mathbf{V}_k^H \mathbf{x}$  (cf. Sec. II-B) and set the linear transform to be  $\mathbf{H} = \mathbf{V}_k^H$ , the input to be  $\mathbf{x}$ , and the estimated output as  $\mathbf{y} = \tilde{\mathbf{x}}_k$ . Again, denote by  $\{\mathbf{x}_t + \mathbf{w}_t\}_{t=1}^{100}$  a stream of 100 noisy realizations of the input process. The statistics of the process and the noise are the same as in Sec. VI-A.

Here we consider a substantially larger problem with an Erdős-Rényi (ER) graph  $\mathcal{G}_{\text{ER}}$  of  $n = 10,000$  nodes and where edges connecting pairs of nodes are drawn independently with  $p_{\text{ER}} = 0.1$ . The signal under study is bandlimited with  $k = 10$  frequency coefficients. To solve the problem (14) we consider the NBH in a4) and the greedy approach in a5). We also consider the case in which the linear transform is sampled directly (Sec. III-B), solving (20) by the greedy approach. Comparisons are carried out against all the methods in b).

In Fig. 4 we show the relative MSE for each method, in two different simulations. First, in Fig. 4a the simulation was carried out as a function of noise  $\sigma_{\text{coeff}}^2$  varying from  $10^{-5}$  to  $10^{-3}$ , for a fixed number of samples  $p = k = 10$ . We observe that the greedy approach in a5) performs best, and the NBH in a4) second. The EDS- $\infty$  in b1) yields the best results among the competing methods. We see that for  $\sigma_{\text{coeff}}^2 = 10^{-5}$  we can obtain a relative MSE of  $5 \cdot 10^{-3}$  by using only  $p = 10$  nodes out of  $n = 10,000$ , *reducing the computational cost of computing the GFT coefficients by a factor of 1,000*. For the second simulation, whose results are shown in Fig. 4b, we fixed the noise at  $\sigma_{\text{coeff}}^2 = 10^{-4}$  and varied the number of samples from  $p = 6$  to  $p = 24$ . Again, the greedy approach in a5) outperforms all the other methods, with the NBH in a4)

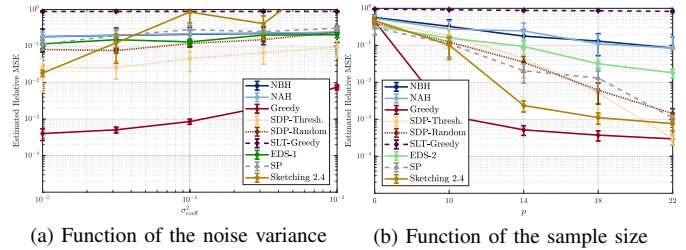


Figure 5. Sensor selection for parameter estimation. Sensor are distributed uniformly over the  $[0, 1]^2$  region of the plane. Sensor graph is built using a Gaussian kernel over the Euclidean distance between sensors, and keeping only 4 nearest neighbors. Relative estimated MSE as: ((a)) A function of  $\sigma_{\text{coeff}}^2$  and ((b)) A function of  $p$ . Legends: SDP-Random (scheme in a1); SDP-Threshold. (scheme in a2); NAH (scheme in a3); NBH (scheme in a4); Greedy (scheme in a5); SLT, EDS-1 and EDS-2 (schemes in b1); SP (scheme in b2); Sketching 2.6, Sketching 2.11 (schemes in c).

as the second best performer. The EDS- $\infty$  in b1) performs better than the SP method in b2). We note that, for  $p < k$ , the EDS- $\infty$  method has a performance very close to the NBH in a4), but as  $p$  grows larger, the gap between them widens, improving the relative performance of the NBH.

In summary, these first two test cases showcased the performance of a (fast) method for computing the GFT coefficients of a collection of streaming, bandlimited graph signals.

### C. Sensor selection for distributed parameter estimation

Here we address the problem of sensor selection for communication-efficient distributed parameter estimation [17]. Let  $\mathbf{x} = \mathbf{H}^T \mathbf{y}$ , where  $\mathbf{x} \in \mathbb{R}^n$  is a vector of sensor measurements (each element is the measurement of one different sensor),  $\mathbf{H}^T \in \mathbb{R}^{n \times m}$  is the observation matrix, and  $\mathbf{y} \in \mathbb{R}^m$  is the parameter to be estimated; refer to [17, Sec. II] for details.

Following [17, Sec. VI-A], we assume that the number of sensors is  $n = 96$ , the number of unknown parameters is  $m = 12$ , and the bandwidth of the sensor measurements is  $k = 10$ . Matrix  $\mathbf{H}^T$  is random where each element is drawn independently following a zero-mean Gaussian distribution with variance  $1/\sqrt{n}$ , as in [17, Sec. VI-A]. The underlying graph support  $\mathcal{G}_U$  is built as follows. Each sensor is positioned at random, according to a uniform distribution, in the region  $[0, 1]^2$  of the plane. With  $d_{i,j}$  denoting the Euclidean distance between sensors  $i$  and  $j$ , their corresponding link weight is computed as  $w_{ij} = \alpha e^{-\beta d_{i,j}^2}$ , where  $\alpha$  and  $\beta$  are constants selected such that the minimum and maximum weights are 0.01 and 1. The network is further sparsified by keeping only the edges in the 4-nearest neighbor graph. Finally, the resulting adjacency matrix is used as the graph shift operator  $\mathbf{S}$ .

For the simulations in this setting we generate a collection  $\{\mathbf{x}_t + \mathbf{w}_t\}_{t=1}^{100}$  of sensor measurements. For each one of these measurements, 100 noise realizations are drawn to estimate the relative MSE defined as  $\mathbb{E}[\|\mathbf{x} - \hat{\mathbf{x}}\|^2] / \mathbb{E}[\|\mathbf{x}\|^2]$ . Recall that  $\hat{\mathbf{x}} = \mathbf{H}^T \mathbf{H}_s^* \mathbf{C}^* (\mathbf{x} + \mathbf{w})$ , with  $\mathbf{H}_s^*$  given by (25) and  $\mathbf{C}^*$  designed according to the methods under study. We run the simulations for 5 different sensor networks and average the results, which are shown in Fig. 5.

For the first simulation, the number of samples is fixed as  $p = k = 10$  and the noise coefficient  $\sigma_{\text{coeff}}^2$  varies from  $10^{-5}$

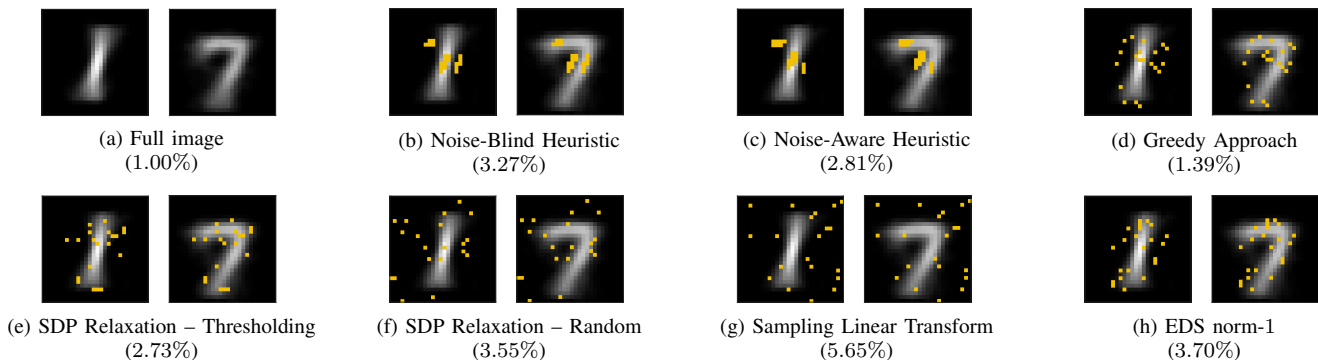


Figure 6. Selected pixels to use for classification of the digits according to each strategy. The percentage error (ratio of errors to total number of images) is also shown. (a) Images showcasing the average of all images in the test set labeled as a 1 (left) and as a 7 (right). Using all pixels to compute  $k = 20$  PCA coefficients and feeding them to a linear SVM classifier yields 1.00% error. (b)–(c) The NAH in a3) and NBH in a4) select a bulk of pixels in places that are the most different between one digit and the other; that is, they select pixels that are mostly white in one digit and black in the other, and viceversa. As expected, the NAH yields slightly better results than the NBH. (d)–(f) Using the greedy approach in a5) or the SDP relaxation in a1) and a2) exhibits a selection of pixels that is more spread out; this is to better account for noise variations. The greedy approach works best, closely followed by the SDP-Thresh. (g) Selected pixels when the linear transform is sampled. (h) Pixels selected by the EDS-1 in b1).

to  $10^{-3}$ . The estimated relative MSE is shown in Fig. 5a. We observe that the greedy approach in a5) performs considerably better than any other method. The solution provided by SDP-Thresh. in a2) exhibits the second best performance. With respect to the methods under comparison, we note that EDS-1 in b1) is the best performer and outperforms NAH in a3) and the NBH in a4), but is still worse than SDP-Random in a1), although comparable. We also observe that while traditional Sketching 2.4 in c) yields good results for low-noise scenarios, its performance quickly degrades as the noise increases. We conclude that using the greedy approach it is possible to estimate the parameter  $\mathbf{y}$  with an accuracy of  $10^{-3}$ , by taking measurements from only 10 out of the 96 deployed sensors.

In the second simulation, we fixed the noise given by  $\sigma_{\text{coeff}}^2 = 10^{-4}$  and varied the number of samples from  $p = 6$  to  $p = 22$ . The estimated relative MSE is depicted in Fig. 5b. We observe that the greedy approach in a5) outperforms all other methods. We also note that, in this case, the Sketching 2.4 algorithm in c) has a very good performance. It is also worth pointing out that the SP method in b2) outperforms the EDS scheme in b1), and that the performance of the SDP relaxations in a1) and a2) improves considerably as  $p$  increases.

#### D. MNIST handwritten digits classification

Finally we consider the problem of classifying images of handwritten digits from the MNIST database [39]. A typical, simple approach to solve this problem, is to compute the PCA transform of each image to be classified, and then feed a few of these PCA coefficients to a linear SVM classifier which will make the final decision [43], [44]. Another option is to exploit the low-rank structure of the data [45]. We note that, when computing the PCA coefficients, the entire image is needed. However, the fact that only few PCA coefficients are required can be understood as the image being bandlimited on the graph given by the covariance matrix. Therefore, under the sketching-as-sampling framework proposed, we can subsume the PCA transform and the SVM classifier (both linear operators) into a single linear transform, and then design

a matrix sketch that would act only on carefully selected pixels, without need to perform calculations on the entire image.

To be more formal, let  $\mathbf{x} \in \mathbb{R}^n$  be the vectorized image, where  $n = 28 \times 28 = 784$  is the total number of pixels. Each element of this vector represents the value of a pixel. Denote by  $\mathbf{R}_x = \mathbf{V}\mathbf{V}^T$  the covariance matrix of  $\mathbf{x}$ . Then, the PCA coefficients are computed as  $\mathbf{x}^{\text{PCA}} = \mathbf{V}^T\mathbf{x}$ . Typically, there are only a few non-negligible PCA coefficients which we assume to be the first  $k \ll n$  elements. These elements can be directly computed by  $\mathbf{x}_k^{\text{PCA}} = \mathbf{V}_k^T\mathbf{x}$  (cf. the GFT, Sec. II). Then, these  $k$  PCA coefficients are fed into a linear SVM classifier,  $\mathbf{A}_{\text{SVM}} \in \mathbb{R}^{m \times k}$  where  $m$  is the total number of digits to be classified. Lastly,  $\mathbf{y} = \mathbf{A}_{\text{SVM}}\mathbf{x}_k^{\text{PCA}} = \mathbf{A}_{\text{SVM}}\mathbf{V}_k^T\mathbf{x}$  is used to determine the class (typically, by assigning the image to the class corresponding to the maximum element in  $\mathbf{y}$ ).

If only few  $k$  PCA coefficients are enough for accurate classification, it means that the image  $\mathbf{x}$  has a subspace representation in terms of the columns of  $\mathbf{V}_k$  (the first  $k$  eigenvectors of the covariance matrix). Following Remark 1, this can be interpreted as the image being a  $k$ -bandlimited graph signal on the covariance graph. This is intuitively satisfying, since it is clear that not all pixels are useful to distinguish between two digits, which suggests that only a few pixels are enough to obtain a complete description of the image (for example, pixels in the borders of the image are always black and pixels that are typically white in both images do not contribute to classification either, see Fig. 6). Then, by modeling the image  $\mathbf{x}$  as a  $k$ -bandlimited graph signal, and by subsuming the PCA transform and the linear classifier in one linear transform  $\mathbf{H} = \mathbf{A}_{\text{SVM}}\mathbf{V}_k^T$ , we can solve this problem of classifying the images of digits by using only a few pixels under the direct sketching-as-sampling framework  $\mathbf{y} = \mathbf{H}\mathbf{x}$ . Finally, we note that while the image is a  $k$ -bandlimited graph signal on the covariance graph  $\mathbf{R}_x$ , this graph is typically fully connected and contains self-loops. We assume, then, that the underlying graph support of the image is actually the precision matrix  $\mathbf{S} = \mathbf{R}_x^{-1} = \mathbf{V}\mathbf{\Lambda}^{-1}\mathbf{V}^T$ , which typically exhibits a

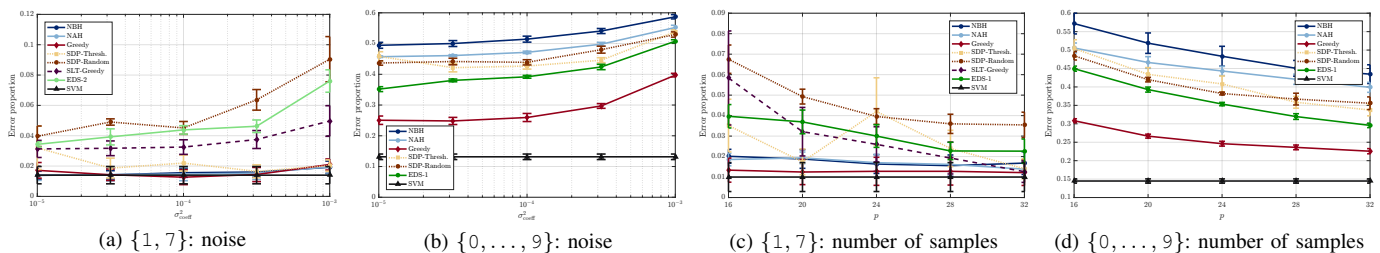


Figure 7. MNIST Digit Classification. Error proportion as a function of noise  $\sigma_{\text{coeff}}^2$  and as a function of the number of samples  $p$ . (a)-(c) Classification of digits  $\{1, 7\}$ . (b)-(d) Classification of ten digits  $\{0, \dots, 9\}$ . We note that in both cases the greedy approach in a5 works best. For two digit classification the worst case difference between the greedy approach and the SVM classifier using the entire image is 0.33%, which happens when attempting classification with just 16 pixels out of 784. For the ten digits case, the difference is 16.36%.

sparse behavior. The image is  $k$ -bandlimited in both  $\mathbf{R}_x$  and  $\mathbf{S}$  since both matrices share the same eigenvectors.

In this experiment, we consider the classification of  $c$  different digits. The MNIST database consists of a training set of 60,000 images and a test set of 10,000. We select, uniformly at random, a subset  $\mathcal{T}$  of training images and a subset  $\mathcal{S}$  of test images, containing only images of the  $c$  digits to be classified. We use the  $|\mathcal{T}|$  images in the training set to estimate the covariance matrix  $\mathbf{R}_x$  and to train the SVM classifier [46]. Then, we run on the test set  $\mathcal{S}$  the classification using the full image, as well as the results of the sketching-as-sampling method implemented by the five different heuristics in a), and compute the proportional error  $e = |\#\text{misclassified images}|/|\mathcal{S}|$  as a measure of performance. We focus on comparing how much the performance degrades by carrying out the classification on only a few pixels (following the sketching-as-sampling framework), as opposed to classifying the digits using the entire image. For all simulations, we add noise to the collection of images to be classified  $\{\mathbf{x}_t + \mathbf{w}_t\}_{t=1}^{|\mathcal{S}|}$ , where  $\mathbf{w}_t$  is zero-mean Gaussian noise with variance  $\mathbf{R}_w = \sigma_w^2 \mathbf{I}_n$ , with  $\sigma_w^2 = \sigma_{\text{coeff}}^2 \mathbb{E}[\|\mathbf{x}\|^2]$  (where the expected energy is estimated from the images in the training set  $\mathcal{T}$ ). We assess performance as function of  $\sigma_{\text{coeff}}^2$  and  $p$ .

We start by classifying digits  $\{1, 7\}$ , that is  $c = 2$ . We do so for fixed  $p = k = 20$  and  $\sigma_{\text{coeff}}^2 = 10^{-4}$ . The training set has  $|\mathcal{T}| = 10,000$  images (5,000 of each digit) and the test set contains  $|\mathcal{S}| = 200$  images (100 of each). Fig. 6 illustrates the averaged images of both digits (averaged across all images of each given class in the test set  $\mathcal{S}$ ) as well as the selected pixels following each different selection technique. We note that, when using the full image, the percentage error obtained is 1%, which means that 2 out of  $|\mathcal{S}| = 200$  images were misclassified. The greedy approach (Fig. 6d) has a percentage error of 1.5% which entails 3 misclassified images, only one more than the full image SVM classifier, but using only  $p = 20$  pixels instead of the  $n = 784$  pixels of the image. Remarkably, even after reducing the computational cost by a factor of 39.2, we only incur a marginal performance degradation (a single additional misclassified image). Moreover, solving the direct sketching-as-sampling problem with any of the proposed heuristics in a) outperforms the selection matrix obtained by EDS-1. When considering the computationally simpler problem of directly sampling the linear transform, the error incurred is of 5.65%. Finally, we note that the sketching-as-sampling techniques

tend to select pixels for classification that are different in each image (pixels that are black in the image of one digit and white in the image of the other digit, and viceversa), i.e., the most discriminative pixels.

For the first parametric example, we consider the same two digits  $\{1, 7\}$  under the same setting as before, but, in one case, for fixed  $p = k = 20$  and varying noise  $\sigma_{\text{coeff}}^2$  (Fig. 7a) and for fixed  $\sigma_{\text{coeff}}^2 = 10^{-4}$  and varying  $p$  (Fig. 7c). We carried out these simulations for 5 different precision graphs (i.e. 5 different random selections of images from the training and test set). For random sampling techniques, a1) and b1), we considered 10 different instances of pixel selection on each graph, and averaged the results. The greedy approach in a5) outperforms all other sketching-as-sampling solutions, and performs comparably to the SVM classifier using the full image. The NAH and NBH also yield satisfactory performance. In the most favorable situation, the greedy approach yields the same performance as the SVM classifier on the full image, but using only 10 pixels, the worst case difference is of 0.33% (1 image) when using only  $p = 16$  pixels (49% reduction in computational cost).

For the second parametric simulation, we consider  $c = 10$  digits:  $\{0, 1, \dots, 9\}$  (Figs. 7b and 7d). We observe that the greedy approach in a5) is always the best performer, although the relative performance with respect to the SVM classifier on the full image worsens. We also observe that the NAH and NBH are more sensitive to noise, being outperformed by the EDS-1 in b1) and the SDP relaxations. This three simulations showcase the tradeoff between faster computations and performance.

## VII. CONCLUSIONS

A problem setup where a collection of high-dimensional signals must be processed using a linear operator was investigated. Assuming that the input signals lie in a low-dimensional subspace, the goal was to develop optimal sampling and sketching schemes to reduce the online processing burden. The sampling scheme selects the subset of input values to be processed, while the sketching scheme specifies the reduced-dimensionality transformation to be applied to the sampled signals. Different from traditional (sampling) schemes aimed at reducing the distortion between the sampled and the original *input* signal, the objective here was to obtain an *output* as close as possible to the one generated by the original (large) linear operator. The joint design problem was formulated as a two-stage optimization where we first found the expression for the

optimal sketching matrix as a function of the sampling strategy and then substituted this expression into the original cost to solve for the optimal sampling scheme. Since the resultant sampling problem was a non-convex binary optimization, different suboptimal schemes were proposed and their complexity was discussed. Simulations using both synthetic and real data demonstrated the merits of the proposed approach.

## REFERENCES

- [1] F. Gama, A. G. Marques, G. Mateos, and A. Ribeiro, "Rethinking sketching as sampling: Linear transforms of graph signals," in *50th Asilomar Conf. Signals, Systems and Comput.*, Pacific Grove, CA, 6-9 Nov. 2016.
- [2] —, "Rethinking sketching as sampling: Efficient approximate solution to linear inverse problems," in *2016 IEEE Global Conf. Signal and Inform. Process.* Washington, DC: IEEE, 7-9 Dec. 2016.
- [3] D. I. Shuman, S. K. Narang, P. Frossard, A. Ortega, and P. Vandergheynst, "The emerging field of signal processing on graphs: Extending high-dimensional data analysis to networks and other irregular domains," *IEEE Signal Process. Mag.*, vol. 30, no. 3, pp. 83–98, May 2013.
- [4] A. Sandryhaila and J. M. F. Moura, "Big data analysis with signal processing on graphs: Representation and processing of massive data sets with irregular structure," *IEEE Signal Process. Mag.*, vol. 31, no. 5, pp. 80–90, Sep. 2014.
- [5] S. K. Narang and A. Ortega, "Perfect reconstruction two-channel wavelet filter banks for graph structured data," *IEEE Trans. Signal Process.*, vol. 60, no. 6, pp. 2786–2799, June 2012.
- [6] A. Sandryhaila and J. M. F. Moura, "Discrete signal processing on graphs: Frequency analysis," *IEEE Trans. Signal Process.*, vol. 62, no. 12, pp. 3042–3054, June 2014.
- [7] K. Slavakis, G. B. Giannakis, and G. Mateos, "Modeling and optimization for big data analytics: (statistical) learning tools for our era of data deluge," *IEEE Signal Process. Mag.*, vol. 31, no. 5, pp. 18–31, Sep. 2014.
- [8] D. K. Berberidis, V. Kekatos, and G. B. Giannakis, "Online censoring for large-scale regressions with application to streaming big data," *IEEE Trans. Signal Process.*, vol. 64, no. 15, pp. 3854–3867, Aug. 2016.
- [9] C. Boutsidis, M. W. Mahoney, and P. Drineas, "An improved algorithm for the column subset selection problem," in *20th Annu. ACM-SIAM Symp. Discrete Algorithms*. New York, NY: SIAM, 4-6 Jan. 2009.
- [10] M. W. Mahoney, "Randomized algorithms for matrices and data," *Foundations and Trends® in Machine Learning*, vol. 3, no. 2, pp. 123–224, 2011.
- [11] D. P. Woodruff, "Sketching as a tool for numerical linear algebra," *Foundations and Trends® in Theoretical Computer Science*, vol. 10, no. 1-2, pp. 1–157, 2014.
- [12] S. Chen, R. Varma, A. Sandryhaila, and J. Kovačević, "Discrete signal processing on graphs: Sampling theory," *IEEE Trans. Signal Process.*, vol. 63, no. 24, pp. 6510–6523, Dec. 2015.
- [13] A. G. Marques, S. Segarra, G. Leus, and A. Ribeiro, "Sampling of graph signals with successive local aggregations," *IEEE Trans. Signal Process.*, vol. 64, no. 7, pp. 1832–1843, Apr. 2016.
- [14] M. Tsitsvero, S. Barbarossa, and P. Di Lorenzo, "Signals on graphs: Uncertainty principle and sampling," *IEEE Trans. Signal Process.*, vol. 64, no. 18, pp. 4845–4860, Sep. 2016.
- [15] A. Anis, A. Gadde, and A. Ortega, "Efficient sampling set selection for bandlimited graph signals using graph spectral proxies," *IEEE Trans. Signal Process.*, vol. 64, no. 14, pp. 3775–3789, July 2016.
- [16] R. M. Gray, "Quantization in task-driven sensing and distributed processing," in *31st IEEE Int. Conf. Acoust., Speech and Signal Process.* Toulouse, France: IEEE, 14-19 May 2006.
- [17] S. Liu, S. P. Chepuri, M. Fardad, E. Masazade, G. Leus, and P. K. Varshney, "Sensor selection for estimation with correlated measurement noise," *IEEE Trans. Signal Process.*, vol. 64, no. 13, pp. 3509–3522, July 2016.
- [18] S. P. Chepuri and G. Leus, "Subsampling for graph power spectrum estimation," in *2016 IEEE Sensor Array Multichannel Signal Process. Workshop*. Rio de Janeiro, Brazil: IEEE, 10-13 July 2016.
- [19] A. Sandryhaila and J. M. F. Moura, "Discrete signal processing on graphs," *IEEE Trans. Signal Process.*, vol. 61, no. 7, pp. 1644–1656, Apr. 2013.
- [20] M. Püschel and J. M. F. Moura, "Algebraic signal processing theory: Foundation and 1-d time," *IEEE Trans. Signal Process.*, vol. 56, no. 8, pp. 3575–3585, Aug. 2008.
- [21] F. R. K. Chung, *Spectral Graph Theory*, ser. Conference Board of the Mathematical Sciences: Regional Conference Series in Mathematics. Providence, RI: American Mathematical Society, 1997, no. 92.
- [22] K. S. Shanmugan and A. M. Breipohl, *Random Signals: Detection, Estimation and Data Analysis*. New York, NY: John Wiley & Sons, 1988.
- [23] B. Girault, P. Gonçalves, and E. Fleury, "Translation and Stationarity for Graph Signals," *École Normale Supérieure de Lyon, Inria Rhône-Alpes*, Research Report RR-8719, Apr. 2015.
- [24] A. G. Marques, S. Segarra, G. Leus, and A. Ribeiro, "Stationary graph processes and spectral estimation," *IEEE Trans. Signal Process.*, vol. 65, no. 22, pp. 5911–5926, Nov. 2017.
- [25] N. Perraudin and P. Vandergheynst, "Stationary signal processing on graphs," *IEEE Trans. Signal Process.*, vol. 65, no. 13, pp. 3462–3477, July 2017.
- [26] S. Segarra, A. G. Marques, G. Leus, and A. Ribeiro, "Space-shift sampling of graph signals," in *41st IEEE Int. Conf. Acoust., Speech and Signal Process.* Shanghai, China: IEEE, 21-25 March 2016.
- [27] S. Segarra, A. G. Marques, G. Mateos, and A. Ribeiro, "Network topology inference from spectral templates," *IEEE Trans. Signal Inf. Process. Netw.*, vol. 3, no. 3, pp. 467–483, Sep. 2017.
- [28] B. Padeloup, V. Gripon, G. Mercier, D. Pastor, and M. G. Rabbat, "Characterization and inference of graph diffusion processes from observations of stationary signals," *IEEE Trans. Signal, Inform. Process. Netw.*, vol. 4, no. 3, pp. 481–496, Sep. 2018.
- [29] M. Mardani, G. Mateos, and G. B. Giannakis, "Subspace learning and imputation for streaming big data matrices and tensors," *IEEE Trans. Signal Process.*, vol. 63, no. 10, pp. 2663–2677, Nov. 2015.
- [30] G. H. Golub and C. F. van Loan, *Matrix Computations*, 3rd ed. Baltimore, MD: Johns Hopkins University Press, 1996.
- [31] W. B. Johnson and J. Lindenstrauss, "Extensions of Lipschitz mappings into a Hilbert space," *Contemporary Mathematics*, vol. 26, p. 189206, Jan. 1984.
- [32] S. Segarra, A. G. Marques, G. Leus, and A. Ribeiro, "Reconstruction of graph signals through percolation from seeding nodes," *IEEE Trans. Signal Process.*, vol. 64, no. 16, pp. 4363–4378, Aug. 2016.
- [33] R. A. Horn and C. R. Johnson, *Matrix Analysis*. Cambridge, UK: Cambridge University Press, 1985.
- [34] S. Boyd and L. Vandenberghe, *Convex Optimization*. Cambridge, UK: Cambridge University Press, 2004.
- [35] G. Puy, N. Tremblay, R. Gribonval, and P. Vandergheynst, "Random sampling of bandlimited graph signals," *Appl. Comput. Harmonic Anal.*, vol. 44, no. 2, pp. 446–475, March 2018.
- [36] A. Frommer and B. Hashemi, "Verified computation of square roots of a matrix," *SIAM J. Matrix Anal. Appl.*, vol. 31, no. 3, pp. 1279–1302, 2010.
- [37] D. E. Knuth, *The Art of Computer Programming*, 2nd ed. Upper Saddle River, NJ: Addison-Wesley, 1998, vol. 3: Sorting and Searching.
- [38] L. F. O. Chamon and A. Ribeiro, "Near-optimality of greedy set selection in the sampling of graph signals," in *2016 IEEE Global Conf. Signal and Inform. Process.* Washington, DC: IEEE, 7-9 Dec. 2016.
- [39] Y. Le Cun, C. Cortes, and C. J. C. Burges, "The MNIST database of handwritten digits," Website, 18 Aug. 2015. [Online]. Available: <http://yann.lecun.com/exdb/mnist/>
- [40] R. Varma, S. Chen, and J. Kovačević, "Spectrum-blind signal recovery on graphs," in *2015 IEEE Int. Workshop Comput. Advances Multi-Sensor Adaptive Process.* Cancún, México: IEEE, 13-16 Dec. 2015, pp. 81–84.
- [41] A. Decelle, F. Krzakala, C. Moore, and L. Zdeborová, "Asymptotic analysis of the stochastic block model for modular networks and its algorithmic applications," *Physical Review E*, vol. 84, no. 6, p. 066106, Dec. 2011.
- [42] D. J. Watts and S. H. Strogatz, "Collective dynamics of 'small-world' networks," *Nature*, vol. 393, no. 6684, pp. 440–442, June 1998.
- [43] J. E. Jackson, *A User's Guide to Principal Components*. New York, NY: John Wiley and Sons, 1991.
- [44] A. K. Jain, *Fundamentals of Digital Image Processing*, ser. Prentice Hall Information and System Sciences Series. Englewood Cliffs, NJ: Prentice Hall, 1989.
- [45] N. Shahid, N. Perraudin, G. Puy, and P. Vandergheynst, "Compressive PCA for low-rank matrices on graphs," *IEEE Trans. Signal, Inform. Process. Netw.*, vol. 3, no. 4, pp. 695–710, Dec. 2017.
- [46] R. O. Duda, P. E. Hart, and D. G. Stork, *Pattern Classification*, 2nd ed. New York, NY: John Wiley and Sons, 2001.